Upwind flight partially explains the migratory routes of locust swarms

Maeva Sorel, Pierre-Emmanuel Gay, Camille Vernier, Sory Cissé, Cyril Piou

HAL Id: hal-04477047
https://hal.inrae.fr/hal-04477047v1

Submitted on 26 Feb 2024
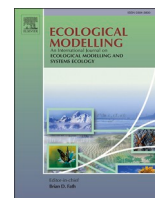
Upwind flight partially explains the migratory routes of locust swarms

Maeva Sorel [a,b], Pierre-Emmanuel Gay [a,b], Camille Vernier [a,b], Sory Cissé [c], Cyril Piou [a,b,*]

[a] *CIRAD, CBGP, F-34398 Montpellier, France*
[b] *CBGP, CIRAD, INRAE, Institut Agro, IRD, Univ Montpellier, Montpellier, France*
[c] *Centre National de Lutte conte le Criquet Pèlerin (CNLCP), Bamako, Mali*

A B S T R A C T

To be efficient, locust swarm control must focus on the place where eggs are laid and hopper bands may appear. But swarms travel a lot and among all the places likely to host them, there is a need to predict to which exactly they will fly. It is then essential to consider movement dynamics to anticipate any displacement that may lead to a further reproduction of locust swarms. Swarms mostly fly downwind and sometimes upwind. We designed an agent-based model to explore swarm displacements depending on the direction of the wind and the possibility for the swarms to realise upwind flights. A primary objective was to assess how upwind flights can improve the replication – and prediction – of documented migratory paths. We looked at the effects of using upwind flight on the swarm ratio arriving in expected (i.e. historically known) areas. Our simulations clearly showed that using upwind flight helped for a better replication of *Schistocerca gregaria* migrations than not using upwind flight. Not using upwind flight reduced swarm dispersion and reduced the range of migrations. Hence, prevailing winds alone cannot explain locust swarm migrations. Food intake must also be considered to regulate movement dynamics and vegetated areas seem to be more attractive to locusts than expected. Our simulations did not perfectly reproduce the general patterns of migrations in some scenarios, but this invites further investigations and the use of other types of field data to calibrate the model. Nonetheless, our results highlighted the importance of upwind flight and showed the major role of wind and temperature on swarm displacement.

1. Introduction

Locusts are an old concern for agriculture around the world. The Bible's Exodus itself referred to a locust invasion as the eighth plague of Egypt (Uvarov, 1944; Kritsky, 1997). Much more recently, swarms of the Desert Locust (*Schistocerca gregaria* Forskål, 1775) invaded Eastern Africa in 2020 (Sultana et al., 2021). Such plagues appear because of a biological specificity of locust species called phase polyphenism (Pener and Simpson, 2009). Under a specific population density threshold, locusts live with solitarious behaviours and do not cause any issue. However, in some conditions, the population is more successful in its reproduction, the density increases, individuals change behaviour and as gregarious the adults start forming swarms. In the Desert Locust, it is when density reaches values between 200 and 1200 adults per hectare depending on vegetation cover, that locusts switch phase from solitarious to gregarious (Cissé et al., 2013). This phase change, or gregarization, is expressed in behavioural, colour, morphological, physiological, and life history changes (Pener and Simpson, 2009). Once, in the gregarious phase, the insects become much more active and

eat and devastate all vegetation on their way.

A good knowledge of the biotopes favourable to population upsurge and phase change is essential for preventive management (Piou and Marescot, 2023). To prevent crises in their early beginning, and because swarms are much harder to eradicate once formed, control measures mainly focus on preventing the apparition of swarms (Magor et al., 2008). Unfortunately, many of the areas where gregarization happen are subject to remoteness such as isolated parts of Sahara or are even in war such as Somalia and Yemen, or insecurity such as some countries in the Sahel, the horn of Africa or the Arabic Peninsula (Showler, 2003). In addition, these countries often suffer from a lack of funds to organise the necessary monitoring despite international assistance through the FAO (Katel et al., 2021). The main consequence is that the Desert Locust still stays one of the major pests in Africa. Because crises still occur, there is a real need to better understand swarm displacement.

Once the swarms are formed, it is essential to forecast their movements in order to anticipate future reproductions that may lead to worsen crisis situation. In addition, the climate change could lead to unexpected and spontaneous migrations towards environments still

---

known to be hostile to locusts (Meynard et al., 2017; CN 2020). Swarm migrations were thus recorded and studied, but available documentation is quite old. Most of the existing scientific articles have been written in 1940s-1980s and were cited in Uvarov's second volume of *"Grasshoppers and locusts"* (Uvarov, 1977). From these, it is known that the locusts' migratory behaviours are strongly influenced by environmental conditions such as wind, vegetation, sunshine and landscape structure (Kennedy, 1951). Intrinsic locust characteristics such as the level of gregarization (gregariousness) and the average age of swarms play also important roles (Kennedy, 1951). Swarms mostly fly downwind but also sometimes upwind (Draper, 1980). These upwind flights often defeat the usual forecasts. Hence, a major challenge in forecasting migration routes of locusts is to consider the role of these upwind flights.

Several agent-based models have been developed to understand phase polyphenism and marching behaviours of hoppers of locusts (Collett et al., 1998; Romanczuk et al., 2009; Yates et al., 2009; Ariel and Ayali, 2015; Dkhili et al., 2017). Some density-based partial differential models were also used to simulate the dynamics of swarms (Topaz et al., 2008; 2012). However, only one model was developed so far with the objective to be able to predict flight direction of swarms in response to environmental conditions: an adaptation of HYSPLIT, an atmospheric particle diffusion model (Stein et al., 2015). The swarm version of this model was not published in the scientific literature and lack an evaluation process. Moreover, upwind flights were not considered nor the specificities of the swarms or their interaction with the vegetation. To fill these gaps, agent-based modelling can be a very interesting approach to simulate swarm migrations considering the swarms characteristics and their interaction with the environment. Such agent-based models built on general concepts and empirical knowledge can bring solid scientific answers especially if they are supported by simulations reproducing field data in a pattern-orientated modelling approach (Grimm et al., 2005). With the development of free and near real-time meteorological and remote sensing data, agent-based models using such environmental data can become very realistic and descriptive of real-world problem (Edmonds and Moss, 2004).

Following this approach, our study objective is to design an agent-based model dealing with locust swarms' migration phenomenon. We wanted to study and consider the cases when swarms can fly upwind. Hence, we developed the model considering downwind and upwind flights as well as the relative frequencies of flying and feeding behaviours depending on the swarm status. During Desert Locust crises in West and North-West Africa in 2004 (Ceccato et al., 2007), and in East Africa and the Horn of Africa in 2019–2020 (Sultana et al., 2021), noticeable swarm movements were documented. Hence, we aim at reproducing the spatial patterns of swarm occurrence observed in these two regions during 8 periods of 2 months, in 2004 and in 2019–2020. The replication of the routes observed during these different periods was a way to compare model versions and parameterisations. Finally, in addition to studying and understanding swarm movement, the present model could become a tool to anticipate migration routes and to adapt control operations accordingly.

2. Material and methods

2.1. Model description

The SANDMAN (*Swarm migrAtion uNder winD, teMperature and vegetAtion iNfluence*) model description follows the ODD (Overview, Design concepts, Details) protocol designed for agent-based and individual-based modelling (Grimm et al., 2006, 2010, 2020). SANDMAN was implemented with Netlogo (Wilensky, 1999), our code is available at: https://doi.org/10.18167/DVN1/1UIN2P .

2.1.1. Purpose and patterns

SANDMAN aims to explore under which wind (direction and speed), temperature and vegetation conditions the swarms of *Schistocerca*

gregaria can fly. The aim is to reproduce the migration routes of swarms observed in West and East Africa respectively in 2004 and 2019–2020. The migration routes shall emerge from the interaction of the swarms with their environment.

2.1.2. Entities, state variables and scales

Entities: SANDMAN consists of two types of entities: the swarms of *Schistocerca gregaria* and the cells representing the environment. Table 1 presents their state variables or attributes.

The swarms are characterised by their geographic coordinates, their surface in km^2 (*Swsize*), their age in days, and their quantity of available energy (*E*) in kcal. These agents are keeping track of their status during the days through some other characteristics: the delays in flight *delay1* and *delay2* are respectively proportions of time not flying due to feeding and unavailable food, *H* is the height of flight, *dist* is the travelled distance and *flightspeed* is the flight speed. The energy states of a swarm are kept in *En* (energy needs), *Em* (energy dedicated to movement), *Ep* (energy dedicated to physiological maintenance), *Es* (energy which can be stored), and *swarmasfood* (energy given by a swarm as a resource in case of cannibalism, expressed in kcal). Additionally, a storage vector of experienced temperature *Vt* per day allows to compute the minimal air temperature at take-off the next day, also stored at the swarm level (*ATD*).

The cells correspond to 10 km by 10 km areas, characterised by air temperature in °C (*T*), wind speed in m/s (*WS*) and wind orientation in degrees (*windorient*: 0° to 360°, clockwise, northward = 0°). The quantity of vegetation present on these 100 km^2 is materialised through a value of NDVI (Normalised Difference Vegetation Index) that corresponds to the difference between the visible red band and the near-infrared band, sensitive to the vigour and quantity of vegetation (Pettorelli et al., 2011). This value is regularly converted as kcal under the name *Ev* (energy resource represented by the vegetation, see § 2.1.7).

Spatial scale: SANDMAN is spatially explicit, in a 1000×450 cells space with finite boundary conditions (non-toroidal world). This environment geographically corresponds to the whole of northern Africa and part of western Asia extending eastwards to India (Fig. 1).

Time scale: The model includes two types of processes, at two different scales. The main time step represents one day, exactly 21 h. Inside, for the second temporal level, we consider 7 periods of 3 h each corresponding to a possibility of displacement. As swarms do not fly by night, the 8th period is not used, because it corresponds to the middle of the night at the intertropical longitudes represented by the model. The typical time horizon of the simulations is 60 days. The 3-hour steps were chosen from the climatic data availability (see § 2.1.6).

2.1.3. Process and scheduling

From this point, the sub-models are abbreviated SM and associated information can be found in Section 2.1.7. The processes are described in Fig. 2. At the beginning of the day and then every 3 h, a process updates the environment cells in terms of wind and temperature, and eventually vegetation (SM1). For a swarm, during a period of 3 h, six functions are called. The first two ones estimate the food requirements of the swarm (SM2) and the resource availability of the cell (SM3). The feeding process only starts when the swarm is hungry. Depending on the previous functions output and if vegetation is available, the swarm feeds (SM4) if vegetation is available. If not, the swarm begins a cannibalism process (SM5) that reduces its size. Sub-model SM6 checks if the conditions are met for take-off and computes in which direction the swarm should go depending on temperature and wind speed. Then, all results of the previous blocks are computed (SM7) in terms of delay due to feeding, orientation and flight speed to determine the actual displacement. All swarms are actualised following these six processes every 3 h. Also, the day temperature is stored for each swarm every 3 h in a list *Vt*. Once the first seven 3 h-periods have passed, *Vt* is used to compute the minimal air temperature at departure for the next day (SM8). Finally, the age of the swarm increases by 1 day.

Table 1

Parameters and selected values.

Name	Type	Value	Description	Sub-Model	Remarks
age	Swarm state	0–60	Swarm age in days	2	
dist	Swarm state	Variable	Distance travelled by a swarm	7	
delay1	Swarm state	*propdelay*, 1	Proportion of the potential distance travelled by a swarm	4	Delay due to time lost for feeding
delay2	Swarm state	Variable	Proportion of the potential distance travelled by a swarm	4	Delay due to lack of resources in the cell
E	Swarm state		Global energy state of a swarm in kcal	2, 4, 5, 7	
En	Swarm state	Variable	Energy needs of a swarm	2	Energy needed to perform an average 3 h-trip
Em	Swarm state	Variable	Moving part of the energy needs	2	
Ep	Swarm state	Variable	Physiological part of the energy needs	2	
Es	Swarm state	Variable	Energy stock possibly made by a swarm	3	
flightspeed	Swarm state	Variable	Flight speed of a swarm	7	
H	Swarm state	Variable	Swarm distance from the ground in m	7	
Swsize	Swarm state	Variable	Swarm size in km^2	2, 5	Value set to 2.8 km^2 for initialisation
Vt	Swarm state	Variable	Vector of experienced temperature over the last 24 h	8	Contains 8 values experienced by the swarm
Ev	Cell state	Variable	Available energy on a patch in kcal	3, 4	Conversion of the vegetation quantity from NDVI
comvbiom	Global	400	Conversion factor to convert biomass (kg) into kcal *Source: Weis-Fogh & Uvarov (1952)*	2, 3	Mean computed within the interval [300, 500]
density	Global	50 000 000	Mean number of individuals per km^2 within a swarm *Source: Rainey (1963)*	2, 5	
meanspeed	Global	4 m/s	Mean flight speed fixed for swarms *Source: Roffey & Magor (2003)*	2, 7	Air speed, mean computed within the interval [3.8, 4.3]
maxspeed	Global	10 m/s	Maximal swarm flight speed	7	

Table 1 (*continued*)

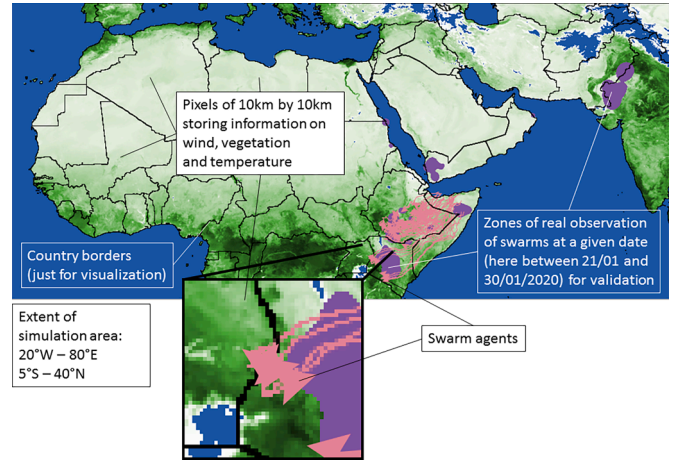| Name	Type	Value	Description	Sub-Model	Remarks
NDVI	Global	0.0–1.0	Quantity of vegetation	3, 4	Updated every 10 or 16 days
WS	Global	Variable	Wind speed in m/s	6, 7	Updated every 3 h loop

Fig. 1. Netlogo's graphical interface of the SANDMAN model. Pixels in green correspond to the vegetation index (NDVI). Pink arrows are the swarms displayed with their trajectories. Validation areas are represented in purple (see § 2.2).
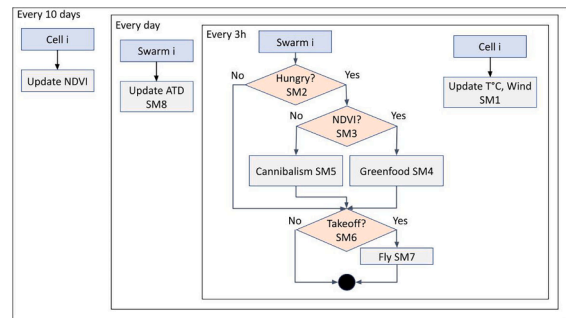

Fig. 2. Organisation of the 8 sub-models. The blue boxes represent the entities, the orange diamonds the Boolean sub-models in which information is stored, and the grey boxes the action sub-models updating variables or making the swarms move (see § 2.1.7).

2.1.4. Design concepts

Basic principles: The model was tuned to reproduce real-world observations of 8 periods, named hereafter "scenarios" (Table 2). For 2004, specific time of the year were considered to focus on large scale movements.

Emergence: the trajectories travelled by the swarms emerge from interaction with environment, and from their movements.

Sensing: swarms perceive the attributes of the environmental cell where they are located: vegetation, temperature, wind speed and wind direction.

Interaction: swarms interact with cells by feeding on available vegetation and thus reduce it. They do not interact with other swarms.

Stochasticity: at initialisation, swarms are generated with random coordinates within a given area. It is the only source of stochasticity in the model.

Observation: every day, the swarms' new computed coordinates

Table 2

List of the real-world observation periods, hereafter named "scenarios". The regions are either Western Africa (WA) or Eastern Africa (EA).

Scenario #	Year	Start date	End date	Region	Coordinates of initialisation*
1	2004	January 1	February 29	WA	(−14, −11, 20, 24)
2	2004	March 1	April 30	WA	(−13, −11, 22, 28)
3	2004	June 1	July 31	WA	(−9, −6, 27, 31)
4	2004	September 1	October 31	WA	(−16, −7, 15, 18)
5	2019	October 1	November 30	EA	(44, 49, 8, 10)
6	2019–2020	December 1	January 31	EA	(44, 49, 7, 11)
7	2020	February 1	March 31	EA	(36, 39, −1, 6)
8	2020	April 1	May 31	EA	(35, 41, −1, 8)

*Initialisation of swarms within a square given by these four coordinates in degrees as: minimum longitude, maximum longitude, minimum latitude and maximum latitude.

trace the displacements. These trajectories allow to compare the results of the simulations with the real-world field surveys at the corresponding periods. To do so, we plotted arrival polygons from field observations and we counted the swarms that reached them after a 10-day period (see Appendix A). This allowed us to assess the performance of our model and validate it. During the displacements, an output variable was tracked (*inrealD*) as a goodness of fit score of the model. It corresponded, each day, to the proportion of simulated swarms present in the places where locusts were observed at the same period (= the expected areas) among the total number of simulated swarms. The higher *inrealD*, the better the model. By construction, *inrealD* varies between 0 and 1. The maps illustrating field observations were generated with the field survey data stored in the FAO's (Food and Agriculture Organization of the United Nations) datasets (see § 2.1.6). The values of *inrealD* were used for the two phases of analyses of the model: a calibration phase where we looked for the parameter values optimising this score for 4 chosen scenarios of two alternative model versions (with and without upwind flight) (§ 2.2), and an exploration phase where we analysed the ability of the best model version (with upwind flight) to reproduce 8 scenarios. The parameters for this model version were chosen according to the calibration phase. During the exploration phase, we also looked at the ratio of upwind flights over the total number of flights performed by the simulated swarms.

2.1.5. Initialisation

The initialisation of the model depends on which of the 8 scenarios we try to reproduce, in two periods of outbreak: years 2004 and 2019–2020. 50 swarms are randomly generated on a given region delimited by a square of minimum and maximum longitude and latitude (Table 2). Swarms have an initial age of zero day, and have an energy reserve to ensure physiological needs for the next 3 h. Their size is set to 2.8 km², which is an average swarm size computed on the FAO dataset (O'Neill, 2020).

2.1.6. External inputs

Wind, temperature: wind data (speed and orientation) at about 200 m above ground level (air layer between 1000 hPa and 985 hPa) and air temperature were downloaded and prepared from the MERRA-2 project (Modern-Era Retrospective analysis for Research and Applications, Version 2) (Gelaro et al., 2017) of the American National Aeronautics and Space Administration (NASA). The MERRA-2 portal is hosted at https://gmao.gsfc.nasa.gov/reanalysis/MERRA-2. Every day and every 3 h steps, these data are entered into the model from raster files.

NDVI: in order to obtain estimates of vegetation biomass we chose NDVI data at 1 km resolution. We used a 10 day-average product: "PROBA-V S10 TOC NDVI 1 KM: Decadal NDVI synthesis of S1's as Maximum Value Compositing" (Roujean et al., 2018) for years 2019–2020. For year 2004, the NDVI was derived from the NOAA MOD13A2 product (Didan et al., 2015) with a temporal resolution of 16 days.

Validation areas: The data used to validate the scenarios were real-world swarm presence maps. These maps contained polygons that we interpolated from the coordinates of swarm recorded during field surveys (see Appendix A). Those polygons delineated the areas with high probability of swarm presence, that we call expected areas. These data were extracted from FAO's Locust-Hub database that stores the national field teams' survey and control results (O'Neill, 2020). Records range from 1985 to 2021; we worked only with the 2004 and 2019–2020 data.

2.1.7. Sub-models

The SANDMAN model includes 8 sub-models.

SM1: Environment update. This first sub-model updates the environmental variables: temperature, wind strength, wind direction and vegetation quantity (NDVI). Temperature and wind data are updated every 3 h. NDVI is updated every 16 days (2003–2013) then 10 days (2014–2020). The maps of expected areas displaying real-world swarm presence are imported every 10 days.

SM2: Hungry? A swarm with not enough energy to move needs to eat. Then, in order to estimate a swarm's hunger, we need to calculate the swarm basic energy needs *En*. We were inspired by the *Dynamic Energy Budget* theory that identifies the allocation of resources in different typical compartments (Kooijman et al., 2008). We considered two requirements: the need for physiological maintenance *Ep*, and the need for movement *Em*, for a 3 h-duration.

$$En = Ep + Em \tag{1}$$

Ep was obtained by monitoring the food quantity consumed by *Schistocerca gregaria* as a function of *age* (Davey, 1954): up to day 5, the amount of biomass consumed increases with *age*. Day 6 and after, this quantity is fixed at 1 g/day, following Davey's observations:

$$food\_quantity = \begin{cases} 0.409 + 0.141 \times age, & if \ age < 6 \\ 1, & if \ age \geq 6 \end{cases} \tag{2}$$

Then, the quantity of food required for physiological maintenance is transformed from g/individual/day to kcal/swarm/3 h:

$$Ep = \frac{food\_quantity \times 0.001 \times Swsize \times density \times convbiom}{4} \tag{3}$$

where *Swsize* is the swarm size, *density* is the number of individuals per km² (in a medium swarm) and *convbiom* is the conversion factor from kg of biomass to kcal. Because it is considered that a swarm cannot fly more than 12 h, the formula is divided by 4, to be related to the 3 h-time steps.

The energy required for the movement *Em* is calculated independently of age, by using the metabolic rate. Weis-Fogh (1952) gave a metabolic rate estimated as proportional (factor 9.8287) to the square of the mean flight speed and expressed in kcal/kg/h. Thus, we convert it to be comparable with *Ep* using this equation:

$$Em = 9.8287 \times meanspeed^2 \times 0.002 \times Swsize \times density \times 3 \tag{4}$$

where 0.002 kg is the average weight of an adult locust (Pélissié et al., 2016). The value is reported to a full swarm as in the previous equation. The factor 3 represents the 3 h-time steps. For a given swarm, when the energy needs *En* is higher than the current state of energy *E*, the Boolean

hungry? is set to true.

SM3: NDVI? Here we check the resources available for a swarm to increase its energy. We first check if there is any vegetation in the cell. To do so, NDVI is converted into energy available for consumption, expressed in kcal, using the following formula, based on Meneses-Tovar's works (2011):

$$Ev = \left(3 \times 10^{-8} \times (NDVI \times 128 + 128)^{4.2473}\right) \times 10^7 \times convbiom \tag{5}$$

In this equation *NDVI* value is converted to tons of biomass per hectare (first part of the equation), and then converted to kilograms with the factor 10^7 and kilocalories using *convbiom*. Vegetation is available when $Ev > 0$, and the result is stored in the Boolean variable *NDVI?*

When feeding, locusts can build up food reserves and store energy (*Es*) for their physiological needs over 2 time periods (6 h overall), plus their movement over the current period:

$$Es = Ep \times 2 + Em \tag{6}$$

When *Ev* is higher than *Es*, the swarm can build up reserves. If not, all the biomass in the cell is consumed. Information about the available quantity of vegetation for feeding is stored in a Boolean variable *enough?*

SM4: Greenfood. This sub-model updates the swarm and the cell state variables representing the food intake on vegetation, and considers the consequences on the displacement. We first set *delay1* as *propdelay* (Tables 1, 3 and 4), as swarms fly for less time because of the time they take to eat. Then, we refer to SM2: if *enough?* is true, the swarm eats its part, then *Ev* and *E* are actualised (by removing *Es* from *Ev* and adding *Es* to *E*). If *enough?* is false, the swarm eats all the vegetation, *E* is updated (by adding *Ev*) but *Ev* is set to 0. In this case, we also compute *delay2*. Because the swarm does not eat according to its needs, it only flies the distance made possible by partial feeding. Thus, *delay2* is calculated as follow:

$$delay2 = \frac{E}{En} \tag{7}$$

Finally, the new *Ev* value is converted into *NDVI* by the inverse function of Eq (5), presented in SM3.

SM5: Cannibalism. This sub-model updates the energy state *E* and *swarmasfood* when locusts eat each other. When no vegetation is available, locust caloric requirements to move remain the same. Cannibalism was already observed in adults of *Schistocerca gregaria* in the case of nitrogen deficiency (van Huis et al., 2008). Thus, locusts can eat each other to achieve sufficient energy to move. An equivalence of the swarm's number of locusts is then transformed in kcal as follow:

$$swarmasfood = 1790 \times 0.002 \times density \times Swsize \tag{8}$$

where we use the factor 1790 to convert a locust in kcal/kg (Van Huis, 2013; Elagba, 2015; Kouřimskáa and Adámkováb, 2016; Mariod, 2020).

Contrasting with SM2 that considers energy storage, cannibalism is the last resort for feeding. Thus, the swarm will only absorb the amount of energy needed for the flight, i.e. the difference between the needed energy *En* and *E* (actual energy available for a given swarm). We then compare this quantity with *swarmasfood*. If the swarm is enough regarding the need (*swarmasfood > En - E*), *swarmasfood* is reduced by the amount of energy required (*En – E*). This loss is then reflected in *Swsize*, in the same proportion as energy loss ($Swsize_{t+1} = Swsize_t - \frac{En-E}{swarmasfood} \times Swsize_t$), and *E* is updated. If the swarm is not enough, or if its size is smaller than 1 km², it dies.

SM6: Takeoff? This submodel first checks if the required conditions to take off are reached. Swarm's take off mainly depends on the local solar time computed from the longitude of swarm's position. Swarms cannot fly at night, between 9:00PM and 9:00AM. The minimum temperature for take-off corresponds to *ATD* (Air Temperature at Departure) (see SM8). In addition, local temperature needs to be higher than a minimum activity threshold (Table 3) and wind may not be too strong (Table 3, below *WSmaxAct*) to allow take off. Temperature and wind conditions also define swarm orientation. Swarms are considered to fly downwind, except in specific situations when temperature is not too high (Table 3, below *Tmax*), and wind is not too strong (Table 3, below *WSmaxFlt*). These parameters are explored in order to adjust flight behaviours during swarm flights (Table 3 & §2.2).

SM7: Fly. Here we compute the results of the previous sub-models in order to define the real distance travelled by the swarms and then make them move. If take off is allowed, swarm flight speed must be calculated and depends on wind orientation.

$$flightspeed = \begin{cases} meanspeed - WS, & \text{if upwind flight} \\ \\ 0.9071 \times WS - 0.199 \times WS^2 + \\ \qquad 0.0049 \times H - 3.7373, & \text{if downwind flight} \end{cases} \tag{9}$$

When swarms fly upwind, we use the average flight speed *meanspeed* (Table 1) and the wind speed *WS*. When swarms fly downwind, they are borne by the wind. Their speed depends on that of the wind, and also on height and temperature. Based on Rainey's works (Rainey, 1963), we used a formula where height (*H*) is computed as a function of temperature obtained by relating height measurements to temperature records (*Tr*) of the same period, obtained from the Berkeley Earth database (Rohde and Hausfather, 2020):

$$H = 76.867 \times (Tr - 20) \tag{10}$$

We set flight speed between 0 and a maximal speed *maxspeed* (Table 1). *flightspeed* is then transformed in km/h with the factor 0.36 and multiplied by 3 flight hours and delays (*delay1* and *delay2*) from the feeding process to obtain an estimate of the distance *dist* travelled during this flight:

$$dist = flightspeed \times 0.36 \times 3 \times delay1 \times delay2 \tag{11}$$

Swarms finally travel a distance *dist* downwind, or upwind using the information *windorient*, in a deterministic way (flight orientation = *windorient* or *windorient* + π respectively). The energy required to perform this flight is then subtracted from *E*.

Table 3
Parameters explored to perform an upwind flight.

Name	Description	Explanations	Tested values
Tmin	Minimal temperature (°C), allowing activity	When temperature is lower, the swarm is cold and cannot move, take off or fly.	[15, 17, 19, 21, 23]
Tmax	Maximal temperature (°C), allowing upwind flight	When temperature is higher, the swarm rises too high, and must be carried by the wind. Thus, it cannot fly upwind.	[25, 30, 35, 40, 45]
WSmaxFlt	Maximal wind speed (m/s), allowing upwind flight	When wind speed is higher, the swarm cannot fly upwind. When upwind flight is impossible this variable is set to 0.	[2, 3, 4, 5, 6]
WSmaxAct	Maximal wind speed (m/s), allowing activity	When wind speed is higher, the swarm cannot take off or fly because of turbulence. When upwind flight is possible, this variable is set to be $\geq WSmaxFlt + 2$	[3, 4, 5, 6, 7]
propdelay	Proportion, giving its value to *delay1* in SM4 and applied to *dist* in SM7	Represents the proportion of the distance that is actually travelled because of delay for feeding	[0.1, 0.25, 0.5, 0.75, 0.9]

SM8: ATD. This sub-model stores daily air temperature every 3 h in a list *Vt*. At the end of the day, it points out the maximum and the minimum and then computes the air temperature at departure *ATD* that will be used the next day, based on the work of Waloff and Rainey (1951):

$$ATD = 5.6 + \left(0.74 \times \frac{min(Vt) + max(Vt)}{2} \right) \tag{12}$$

2.2. Simulations

As explained in "Basic principles", we used 8 scenarios to adjust and explore the model's outputs (Table 2). As seen in SM6, the parameters related to flight possibility and direction were explored to evaluate the role of upwind flights in locust migration (Table 1). Other factor explored was the delay due to feeding *propdelay*.

We used two versions of our model SANDMAN in order to determine if upwind flights affect the quality of the predictions. In a first version (IUF, *Impossible Upwind Flight*), we prevented any swarm movement against the wind by deactivating the process of upwind flight: parameters *WSmaxFlt* and *Tmax* were set to 0. Conversely, in the PUF (*Possible Upwind Flight*) version, these two parameters were activated, so swarms could fly against the wind. In this last version, we constrained the exploration by forcing a difference of 2 m/s between *WSmaxFlt* and *WSmaxAct* to unsure that actual upwind flights could be possible.

In a calibration phase, for each version of the model, we simulated five replicates for 4 real-world scenarios (scenarios number 3 and 4 in 2004, and 6 and 7 in 2019) using combinations of 5 values per parameter (Table 3). For each run we recorded *inrealD* values (see § 2.1.4) for the last 10 days of the scenarios to focus on the arrivals of flights after 60 days. We kept the parameter values which maximised the *inrealD* score in two different ways. In the first way (thereafter called "Compr."), we allowed the best compromise across the whole set of scenarios, trying to

maximise the *inrealD* score as a mean of the results across all scenarios. In the second way (thereafter called "Best"), we used the parameters that maximised the scores for each tested scenario. We compared the *inrealD* scores between both versions of the model, by type of maximisation method and scenarios.

In the exploration phase, we evaluated the efficiency of SANDMAN as a migration simulator for the 8 scenarios using the PUF version with the set of parameters values obtained with the compromise method (Compr.) in the calibration phase. We extracted the coordinates of the swarms every 10 days. We sorted these coordinates using 5 randomised simulations by scenario as previously, for every scenario. These coordinates were reported on a map with the R software (The R Project for Statistical Computing, n.d.), with the positions recorded in the FAO dataset at the same periods. This visualisation allowed to compare the simulations and the real positions recorded across time, and to evaluate them as regards of typical migration patterns (Waloff, 1966). To evaluate the importance of upwind flights, we recorded the ratio of upwind flights over the total number of flights performed by the simulated swarms in the 8 scenarios.

3. Results

3.1. PUF and IUF calibration and comparison

We looked at the effects of upwind flight on the swarm ratio in the expected area at the end of the simulation by comparing Possible upwind flight (PUF) and Impossible upwind flight (IUF) model versions. Focusing on the optimisation by scenario (Best in Fig. 3), the possibility of upwind flight (PUF) always reached higher or equivalent results than IUF. The proportion of simulated swarms found in the areas where they actually were present in both PUF and IUF models are close in Sc. 3 and

Table 4
Parameters obtained during the calibration phase on 4 scenarios (see Table 3 for parameter description) for the two model versions (PUF = Possible Upwind Flight; IUF = Impossible Upwind Flight).

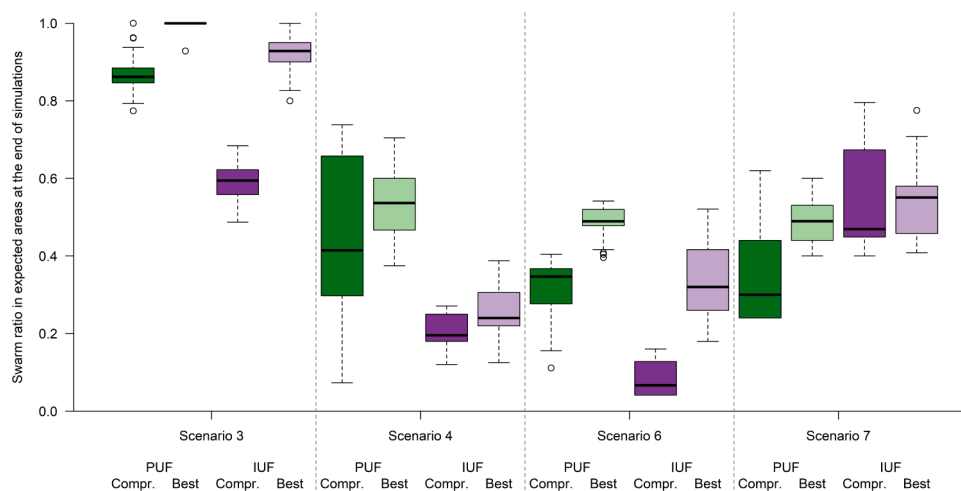| Name	Tested values	Best Sc. 3 PUF	IUF	Best Sc. 4 PUF	IUF	Best Sc. 6 PUF	IUF	Best Sc. 7 PUF	IUF	Compr. PUF	Compr. IUF
Tmin	[15, 17, 19, 21, 23]	19	19	17	23	23	17	23	23	23	19
Tmax	[25, 30, 35, 40, 45]	45	0	45	0	40	0	45	0	45	0
WSmaxFlt	[2, 3, 4, 5, 6]	5	0	2	0	4	0	2	0	3	0
WSmaxAct	[3, 4, 5, 6, 7]	7	6	4	3	7	5	4	3	5	3
propdelay	[0.1, 0.25, 0.5, 0.75, 0.9]	0.25	0.1	0.9	0.25	0.9	0.25	0.5	0.75	0.25	0.1

Fig. 3. Swarm ratio in expected areas at the end of the 60-day simulations obtained in the two versions of the model. Possible upwind flight in green (PUF). Impossible upwind flight in purple (IUF). Proportions are computed under two sets of parameter values: one optimised across all scenarios (Compr., dark green and dark purple boxplots) and one optimised for each scenario (Best, light green and light purple boxplots). Scenario 3 started in Jun. 2004, Sc. 4 in Sep. 2004, Sc. 6 in Dec. 2019 and Sc. 7 in Feb. 2020 (Table 2).

7, and clearly higher in Sc. 4 and 6. Focusing on the compromised optimisation (Compr. in Fig. 3), the proportions obtained for the PUF model version gave higher results in Sc. 3, 4 and 6 than the IUF model version. Conversely, the IUF results were higher in Sc. 7. Excepted in this last case, the PUF model version always gave equivalent or better results of swarm localisation than the IUF model version (Fig. 3). The best parameters for the different scenarios for PUF were often selecting the maximum Tmax value (45 °C) except in the case of scenario 6 (Table 4). The set of parameters to optimise all scenarios (Compr.) with possible upwind flight (PUF) selected the maximum *Tmin* and *Tmax* values, intermediate *WSmaxFlt* and *WSmaxAct* and a low value of *propdelay* (Table 4). The corresponding parameter set optimising all scenarios with impossible upwind flight (IUF) selected an intermediate value of *Tmin* and the lowest values for *WSmaxAct* and *propdelay*.

3.2. Exploration by confronting the model to real data

3.2.1. First period (Sc. 1–4, 2004)

The first period focused on a plague that occurred in the North-West of Africa in 2003–2004, that is considered in scenarios 1 to 4.

In Sc. 1 and 2, according to the real data, the swarms were not supposed to migrate for a long distance. The simulations did reproduce the expected migrations. Swarms remained present on the initialisation area in Mauritania throughout the whole simulation time. The model resulted in a very little movement only in Mauritania and Western Sahara, which corresponded to what was expected for these two scenarios (Appendix B). Conversely, in Sc. 3 and 4, real data showed significant migration, northwards (Sc. 4) and southwards (Sc. 3). In Sc. 3, even if the simulated swarms did not reach the exact area where they were expected, the direction of the southward migration was respected (Fig. 4). In Sc. 4, the simulated swarms remained stuck in the initialisation area in the south of Mauritania and Senegal, where records were present during the whole period of simulation, but they did not move northwards as it was expected regarding real data.

3.2.2. Second period (Sc. 5–8, 2019–2020)

The second period focused on a plague that affected Eastern Africa in December 2019 and 2020 and went on until the end of 2021, that is considered in scenarios 5 to 8 (Appendix C).

In Sc. 5, the real records indicated a short migration event from the Horn of Africa towards the Somalian-Ethiopian border and the appearance of more swarms near the Gulf of Aden. The simulated swarms actually moved westwards, but also southwards. In Sc. 6, the real data showed a large migration event from the North-East to the South-West,
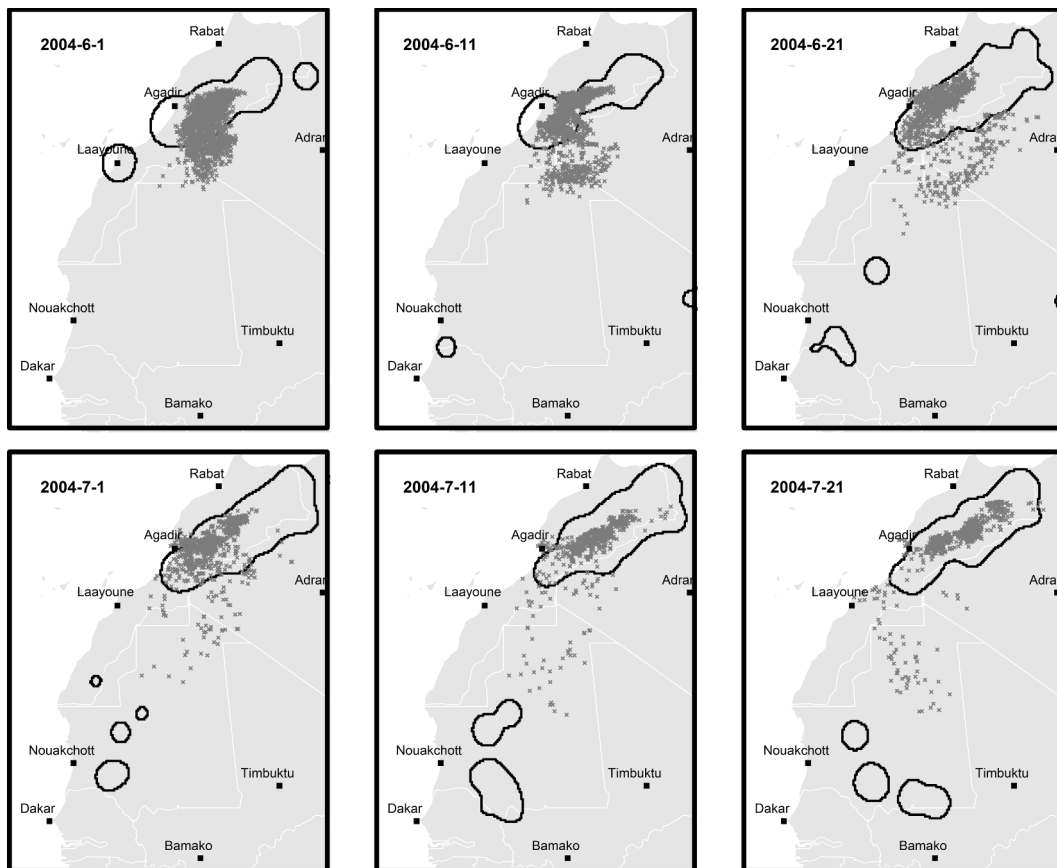

Fig. 4. Comparison map between FAO swarm records (black polygons) and SANDMAN simulated swarms (dark grey dots), run with the Possible Upwind Flight version using the parameter set selected with the compromise method (see §2.2). Computed from scenario 3 (Table 2). From left to right, the pictures were taken every 10 days, from June 1 to July 30, 2004.
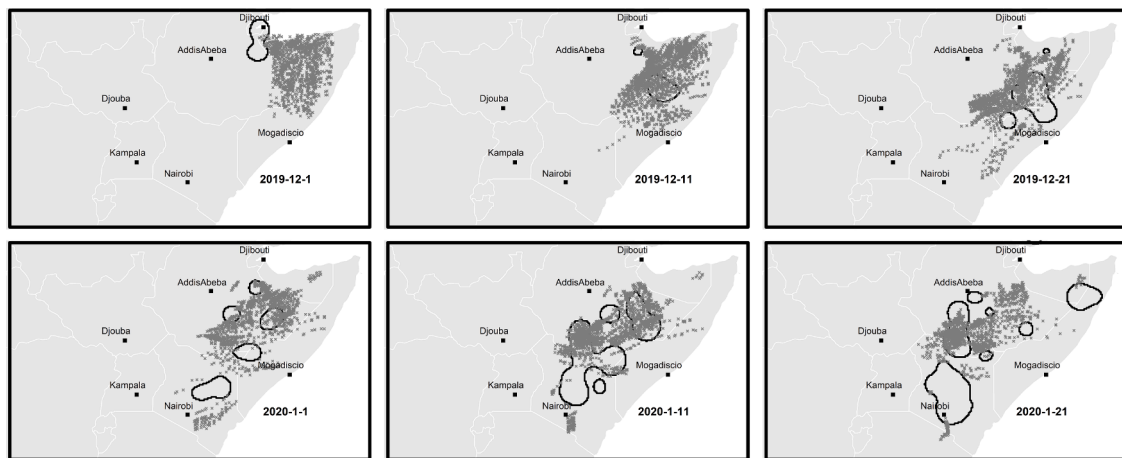
Fig. 5. Comparison map between FAO swarm records (black polygons) and SANDMAN simulated swarms (dark grey dots), run with the Possible Upwind Flight version using the parameter set selected with the compromise method (see §2.2). Computed from scenario 6 (Table 2). From left to right, the pictures were taken every 10 days, from Dec 1, 2019 to Jan 31, 2020.

across the area around the Ethiopian-Somalian boundary, up to Kenya. The simulated swarms followed this pattern, following a dispersion movement from East to West (Fig. 5). In Sc. 7 and Sc. 8, the expected migration events were short: the real data showed a dispersion from East to West following the trend of Sc. 7 and almost no movement in Sc. 8. In both cases, the simulated swarms migrated too far and too fast westwards, reaching areas such as the Democratic Republic of Congo (Sc. 7) or the South and even the North of Sudan (Sc. 8), where there was no record.

The upwind-flights of swarms during the simulations of the 8 scenarios were ranging from 20% to 60% of the total performed flights (Appendix D), with more variations among than within scenarios. This result from the specific wind regimes and temperatures for each scenario.

4. Discussion

The objective of this study was twofold: i) build an integrative model from the literature on locust swarm movement and ii) evaluate its quality using simulations. With the development of this model, we could assess the influence of previously defined factors and processes affecting swarm movement. Our simulations clearly showed that upwind flight must be considered for a better replication of *Schistocerca gregaria* migrations. Locust sometimes show such behaviours which are not prevailing, so we had to integrate them into the model to reproduce reality. These results are consistent with the assumption that the flight routes are emerging from the interaction of locusts in the swarm with their environment in order to avoid inappropriate and dangerous areas as much as possible, particularly during low altitude flights (Shashar et al., 2005). During the parameterisation process, the retained values for the upwind flight version of the model can be discussed in the light of desert locust literature. We address the importance of upwind flights in a first part of the discussion. In a second part, we discuss the representativity of the model in front of real-world observations. A third part discusses the large-scale constraints in modelling ecological processes. And a last part opens the discussion on the improvement of preventive management of desert locust.

4.1. Upwind flight matters

Desert locusts fly most of the time downwind, but they can also choose to fly upwind under certain conditions: light wind speed, rain in sight, or high ground (Draper, 1980; Symmons and Cressman, 2001). Even if upwind flight constitutes a small part of all flights, we added this ability to the model in order to better match locust behaviour. The comparison of the two versions of SANDMAN, computed with two optimisation methods, delivered either better or equivalent results when upwind flight was allowed, in 3 out of 4 scenarios with the exception of Sc. 7 (optimised with compromise). The maps of the 8 scenarios with the impossible upwind flight version (Appendix E) show also lower or equivalent quality of reproduction of the overall trajectories than with the possible upwind flight version (Figs. 3 and 4 and Appendices B and C). Not allowing upwind flights reduces swarm dispersion and reduces the range of migrations in SANDMAN. We also saw in our simulations that upwind flights could occur in SANDMAN up to 60% of the cases, depending on the scenarios (Appendix D). These results not only highlighted the importance of upwind flight in the replication of migrations, but also can be interpreted as a dependence on wind and temperature factors. We built the model's relationship from the literature, and then we refined the parameter values to match the real-world patterns from different situations. However, we could not entirely validate the parameter values because of the few information available in the literature or real data. The retained values for the upwind flight version of the model are comparable to some old literature information. For example, the 5 m/s maximum wind speed allowing flight is relatively low in comparison to the conditions of swarm flights observed by Waloff (1972) of sometimes up to 7 m/s wind speed at 2 m during swarm flight. The 3 m/s maximum wind speed that allows upwind flight is realistic compared to Weis-Fogh's (1956) tunnel assays measurements of maximum desert locust flight speed between 3.5 and 4.2 m/s. The 23 °C minimum temperature of activity is quite high in comparison to some observations of air temperature at departure below 20 °C by Waloff & Rainey (1951). Finally, the 45 °C maximum air temperature allowing upwind flight corresponds to a flight approximately at a height of 2000 m, which has already been observed (Rainey and Waloff 1951). These small discrepancies between the literature and our results illustrate that further research in swarms' flight conditions and on individual locust

flight behaviours would probably improve the realism of the model.

In particular, we failed to reproduce the movement expected in Sc. 4 (swarms travelling from South to North in West Africa). And yet this trajectory is one of the best known regarding *Schistocerca gregaria* (Symmons and Cressman, 2001; FAO, n.d.1). This area, at the relevant period, showed particular environmental conditions: strong warm air currents blowing from the Sahara, associated with an atmospheric depression over the western Mediterranean, helped swarm flight (Cressman and Stefanski, 2016). The locusts thus waited for warmer winds blowing from the South instead of using the prevailing cooler winds blowing from the North. We actually did observe such a movement with SANDMAN, but during relatively short times and this was not enough to reproduce the swarm displacement that was observed in the field. One of the hypotheses we can put forward is that under those specific conditions, the swarms would be able to cover greater distances than we had anticipated. But it remains to be determined how and in which conditions. Another hypothesis is that locust flight is much more complex than current knowledge suggests. For instance, our model does not consider the role of thermal breezes. These coastal and local winds are caused by the difference in temperature between land and sea. They are independent of the general regime of winds and blow on a narrow coastal strip. At night and in the morning, they blow from the land to the sea, taking locusts off, then during the day from the sea to the land, driving them back towards the coast. According to the locust control services of Mauritania, this phenomenon has been observed many times, but was not documented and only orally spread in form of anecdotes. The locusts were thus able to benefit from the cyclic succession of these contrary winds regularly sending them in the opposite direction, to progress gradually northwards along the coast. This phenomenon would explain that the model did not reproduce in Sc. 4 the movements from Mauritania towards Morocco following the coast, that are yet well known and documented (FAO, 2004, n.d.2). Another question needs to be answered: apart from being sensitive to warmer temperature, what really motivates locusts to fly in the presence of strong headwinds? Could it be the perception of moisture brought by the wind? Or the sight of greenness? Or the perception of colours, even basic? There is a lot to be asked about and to launch further studies on this subject. This will no doubt help greatly in understanding locust movement.

4.2. Representativity of the simulation outcomes

The modelling of the swarm energy limits is inspired by the *Dynamic Energy Budget* theory (van der Meer, 2006; Kooijman, 2009) and allows to predict realistic travelled distances related to food intake. We confirmed that the effects of these energy limits are not artefacts, since swarms could move slower than expected (Sc. 4), or conversely be beyond the forecast (Sc. 7 and Sc. 8) where the swarms moved too fast and too far. The potential reasons why the model behaved differently (absence of swarm movement from coastal Mauritania to Morocco) from the empirical observations of Sc. 4 have been given earlier (§ 4.1), but we did not explain the scenarios in 2019–2020 when swarms moved too far. We talked previously about the migrations, whose main patterns mostly concern displacement between reproduction areas. With regard on this last point, our best lead explaining an excess of mobility would be an under-estimated attraction of the vegetated areas: in addition to being useful for feeding, these areas are a key element in the reproduction process (Roffey and Popov, 1968; Cissé et al., 2013; Maeno et al., 2020), which is not considered in SANDMAN. As a result, vegetated areas are probably much more attractive than we had modelled. In particular, the observed migration patterns follow the seasonality of

vegetated areas in a way that they are synchronised with the reproductive cycles (Symmons and Cressman, 2001). In order to accurately represent such a process, it would be necessary to integrate an additional layer of memory effect (i.e. the more vegetated areas a swarm finds, the faster it becomes able to find more), including a set of processes involved in the population dynamics.

The scenarios were evaluated with maps of expected areas (Appendix A) but these maps could be hard to assess when looking at the scores if the relevant areas are too fragmented. This is why we did not only consider the scores but also the whole trajectory when confronting to real data. This way, we can have a more global evaluation of SANDMAN's results, and we can also identify other explanations about the trajectories a bit far from what we expected. A main bias concerns the field observations. First, FAO dataset does not individually follow each swarm and does not distinguish different swarms in the same place. Second, SANDMAN does not include any population dynamics process, so we considered changes in the maps of FAO data as swarm displacement. Our model also did not consider swarm reproduction while data actually includes young swarms that have just emerged. That means that we cannot know if a swarm notification concerns a new swarm that has just emerged or the movement of a previous one. Also, the cohesion level within a swarm could influence direction changes during flight (Edelstein-Keshet et al., 1998; Murakami et al., 2017; Yates et al., 2009). Such details are not given by the FAO dataset. Further analyses and consideration of the different sources of uncertainties could improve the calibration of SANDMAN. Dataset following specific swarms would enhance greatly this and could be the objective of further studies.

4.3. Modelling large scale processes with agent-based models

Swarm movement has already been modelled for forecasting purpose, but was processed as particle diffusion, as in the model HYSPLIT developed by the NOAA/Air Resources Laboratory, one of the most widely used models to follow dispersion of atmospheric pollutants (Stein et al., 2015): all swarms reacted similarly to their environment, with no distinction. Conversely, we used here agent-based modelling in order to add specific history and behaviour to each swarm. We modelled migrations as a result of environmental data, the physical limits of the insects, and some biological processes reflected with the Dynamic Energy Budget (Van der Meer, 2006). In this way, SANDMAN can more accurately predict the movement of swarms that have already been formed, using the same input information as other standard models.

Large-scale individual-based models have been proposed quite early in the ecological modelling literature (e.g. Cary et al., 1992). Nevertheless, spatial processes at the continental scale are rarely implemented in agent-based models in ecology. Parry and Bithell (2012) differentiate two approaches to scaling up geographical processes in agent-based models: the super-individual approach and a multi-core hardware parallelisation (to increase the number of agents and/or the spatial extent). We used here a super-individual approach that allowed a potential gain of efficiency in term of computing speed and memory use. Our approach using remote-sensing and climatic models' information at the scale of continents allowed us to focus on the interaction of the swarms as super-individuals to large scale climatic processes (wind, temperature and vegetation). Swarm behaviours are typically studied by analysing group movements emerging from individual interactions (e.g. Dkhili et al., 2017). However, the large-scale aspect of desert locust swarm migrations makes hard the analysis of processes at the level of the individual. Given the scale at which we need to consider our model, our approach is a good compromise between tractability and complexity of

the model.

Agent-based models in ecology should consider individual-environment interactions to let emerge large-scale processes in order to investigate ecosystem and community ecology questions (Grimm et al., 2017). This approach has been widely accepted in population ecology and proposed by Huston et al. (1988) to unify ecological theory. When using a super-individual approach, we can still represent environment-individual interactions and demographic processes. However, the inter-individual interactions are lacking. An approach of comparison of small and large-scale models using respectively individuals and super-individuals could improve the realism of the super-individual ABMs, eventually even by calibrating these models with the outcomes of the small-scale models. Further efforts could be done in this direction, and locust questions are perfect examples of potentially benefiting problematic from such approaches.

4.4. Improving preventive management

Knowing and understanding swarm displacement is essential in curative locust control in general and in preventive control in particular. Preventive control in an upsurge context consists in anticipating where the swarms are going to move before they lay eggs, in order to despatch control teams on the spot and thus eliminate nymphs before imaginal moulting and further multiplication. Our model, based on the observation of pathways and modes of displacement of locusts observed for decades, is an additional tool to anticipate the evolution of an emerging crisis situation. Many other tools in early warning systems (Magor et al., 2008; FAO, 2022) can be used to determine suitable areas for population clusters and reproduction: characterisation of biotopes, monitoring of rainfall, remote sensing (NDVI, soil moisture), etc. (Cressman, 2008, 2013; Gómez et al., 2019; Piou et al., 2013, 2019; Piou and Marescot, 2023). But it remains to discern among all these favourable areas the ones towards which the swarms will go. At this level, the experience of the anti-locust field teams is of course paramount (Gay et al., 2021). A tool such as that prefigured by SANDMAN or its possible further development, which allows to predict swarm movements by performing simulations using all types of winds, is a real plus for preventive control.

Finally, contrary to common belief, considering that locust swarms can sometimes fly upwind significantly improves prediction accuracy and proposes some explanations for some displacements that are historically known and documented, but were not following the prevailing winds.

CRediT authorship contribution statement

Maeva Sorel: Conceptualization, Formal analysis, Investigation, Writing – original draft, Writing – review & editing. **Pierre-Emmanuel Gay:** Data curation, Writing – review & editing. **Camille Vernier:** Writing – review & editing. **Sory Cissé:** Writing – review & editing. **Cyril Piou:** Conceptualization, Formal analysis, Investigation, Methodology, Project administration, Resources, Supervision, Writing – review & editing.

Declaration of competing interest

The authors declare that they have no known competing financial interests or personal relationships that could have appeared to influence the work reported in this paper.

Data availability

The source code is available online. https://doi.org/10.18167/DVN1/1UIN2P

Appendix A

In order to draw the maps of real-world swarm presence, it was first necessary to retrieve the FAO data (O'Neill, 2020), that are spatialised. Each swarm record had its own coordinates: latitude and longitude. These data were also associated with dates. In order to obtain more general trajectories, we grouped the data into 10-day periods and we cumulated the records.

These data, in the form of coordinates, were then transformed in two steps: first, they were changed into a set of 2-dimension spatialised points, i.e. a point process (ppp object of the R Spatstat package (Baddeley et al., 2015)). This allowed to get a distribution map of swarms in Africa and in South West Asia. Second, we converted these point processes into densities. We used a Gaussian kernel with a standard deviation of 0.5° to obtain the density of points in the whole map with the function « density.ppp » of Spatstat. This conversion resulted in a concentration gradient of the swarm records across the entire map on pixels of 0.5° (see Piou et al. (2017) for an example of this methodology). We then transformed this rasterised information into polygons where at least one swarm could be found, the rest of the map being considered swarm-free.

In this way, we produced polygons for each 10-day period corresponding to the scenarios used in the simulations.

Appendix B

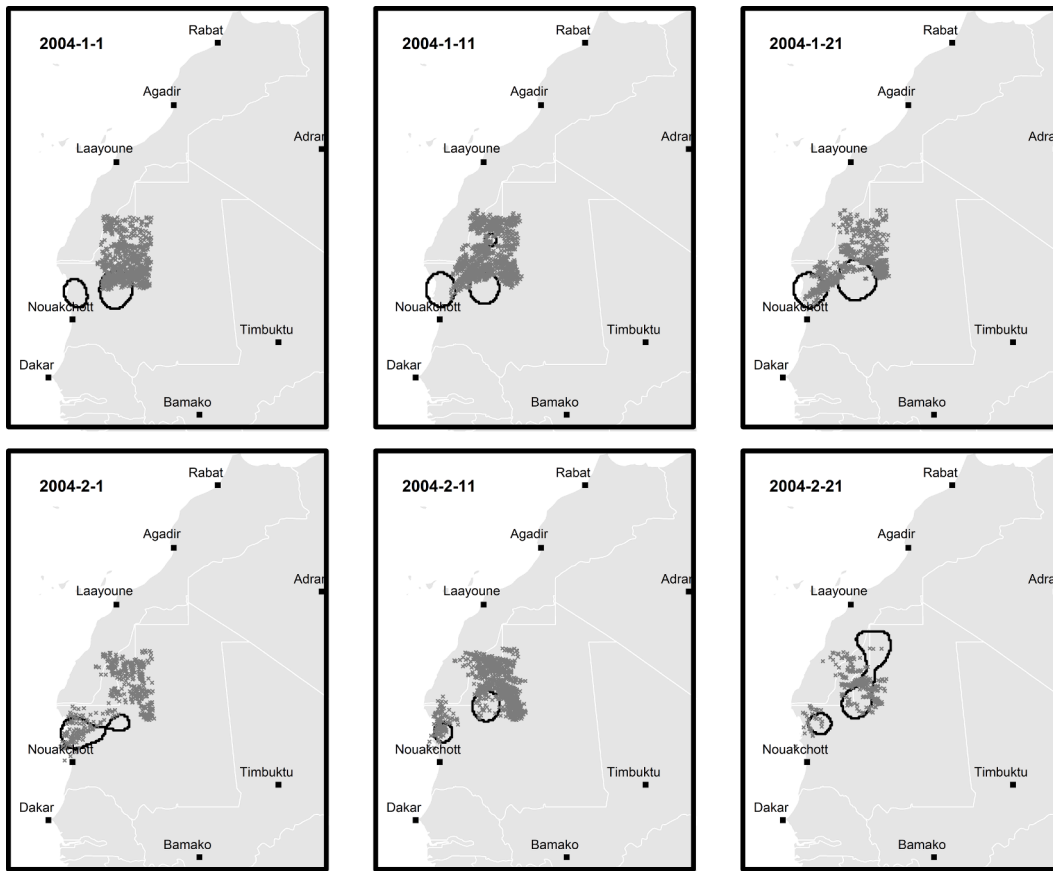(Fig. B-1, Fig. B-2, Fig. B-3)
Scenarios 1, 2 & 4, Western Africa, 2004.

Fig. B-1. Scenario 1, Jan.-Feb. 2004.

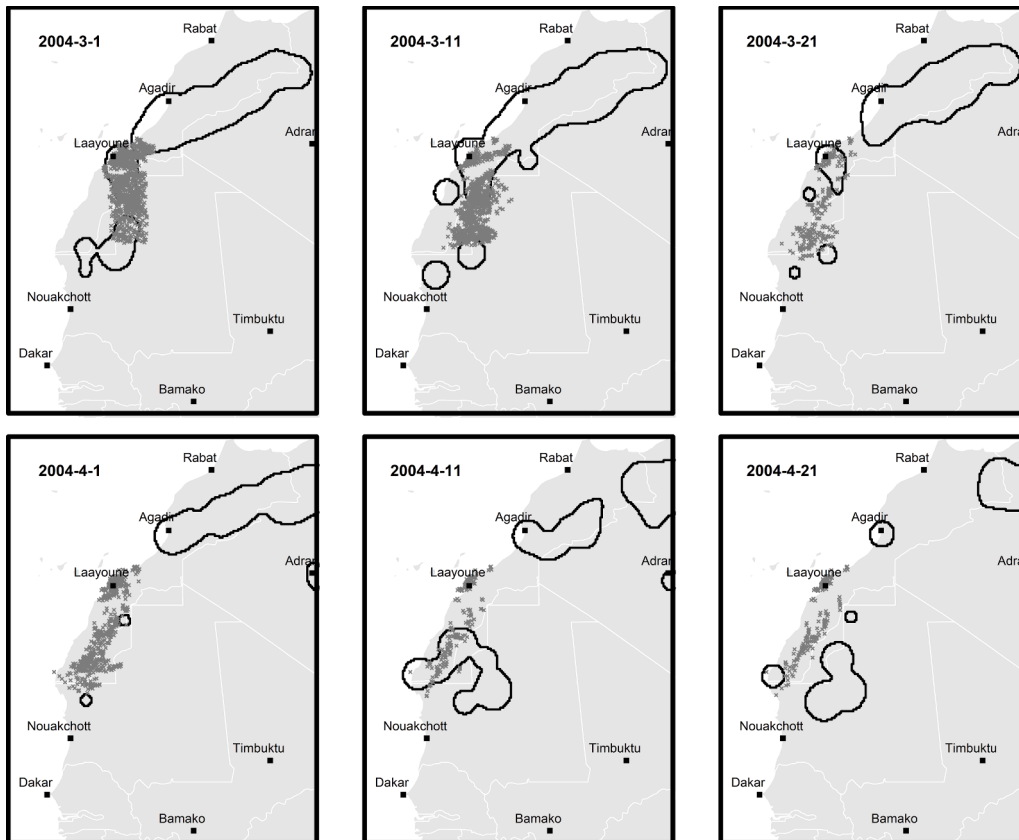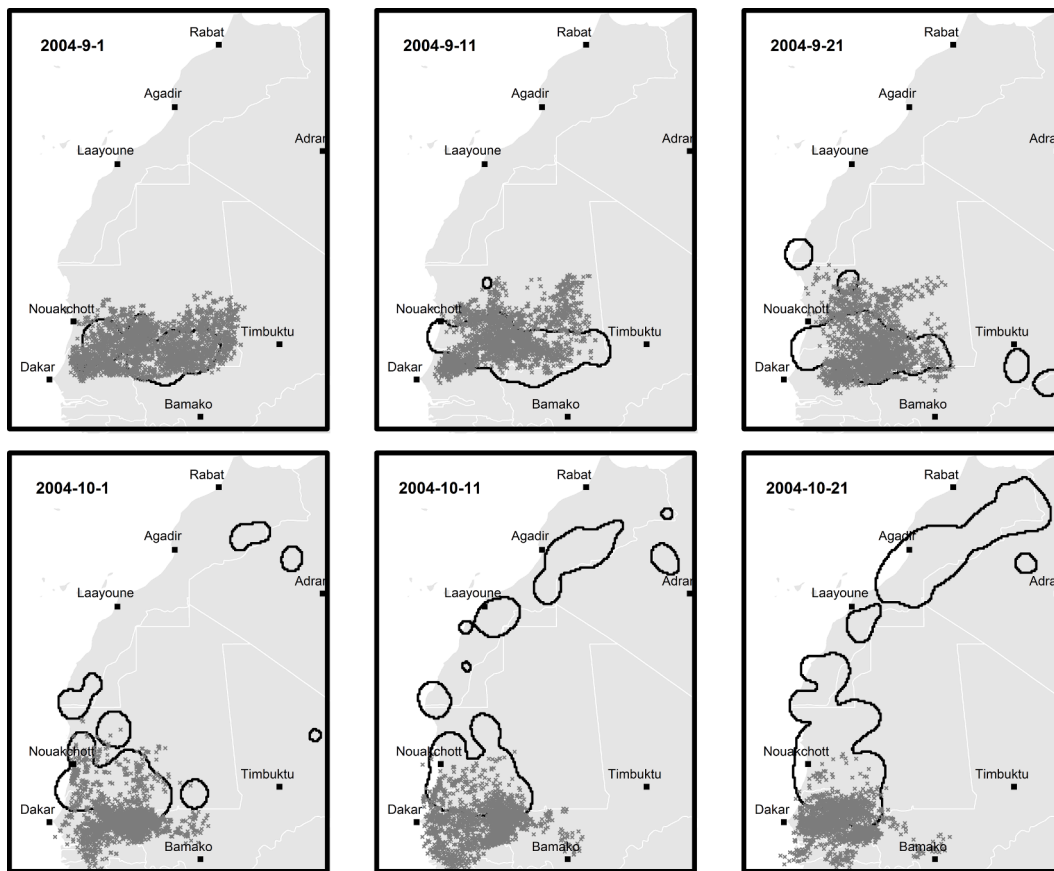**Fig. B-2.** Scenario 2, Mar.-Apr. 2004.

Fig. B-3. Scenario 4, Sep.-Oct. 2004.

Appendix C

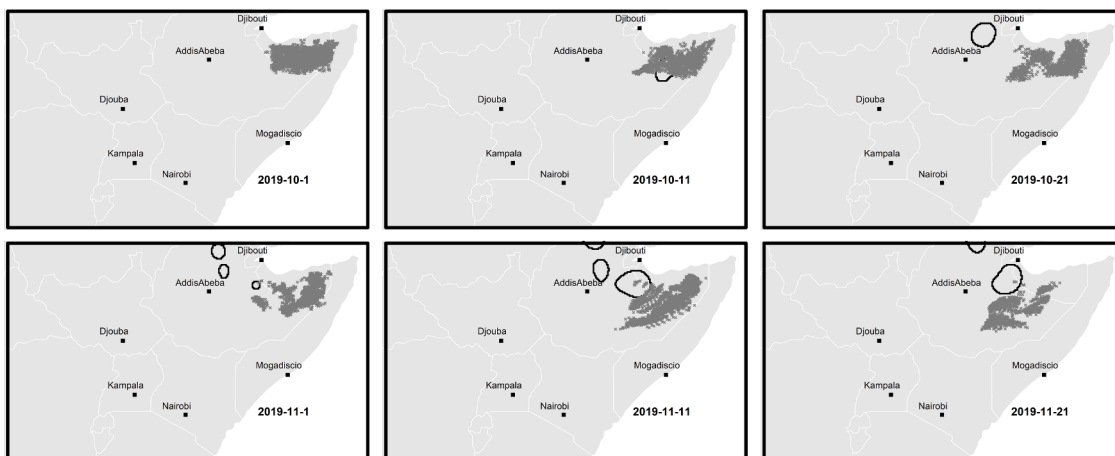Scenarios 5, 7 & 8, Eastern Africa, 2019–2020.

Fig. C-1. Scenario 5, Oct.-Nov. 2019.
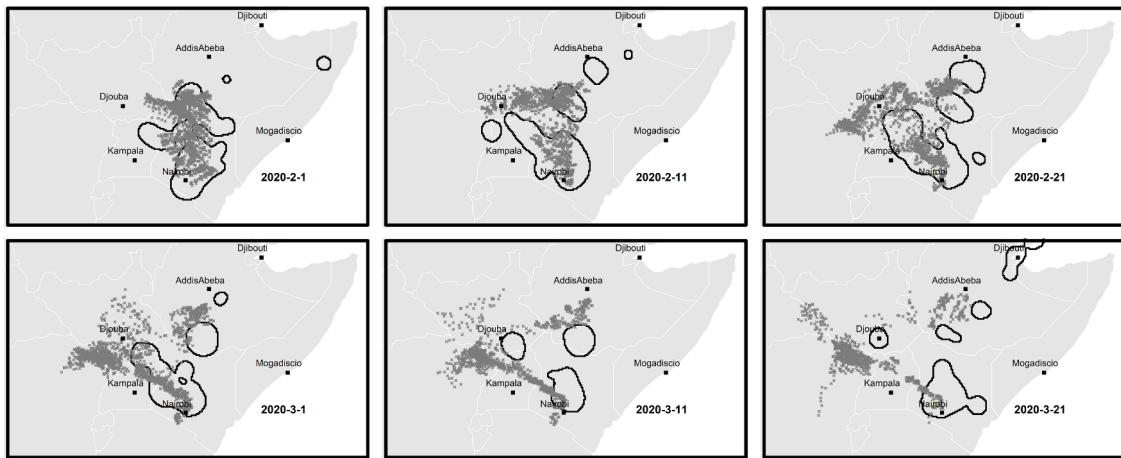
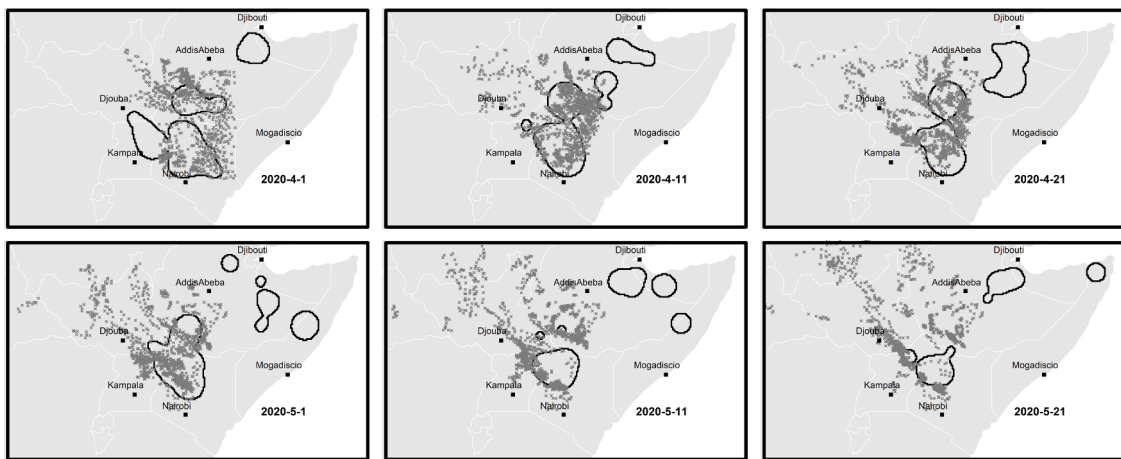**Fig. C-2.** Scenario 7, Feb.-Mar. 2020.

Fig. C-3. Scenario 8, Apr.-May 2020.
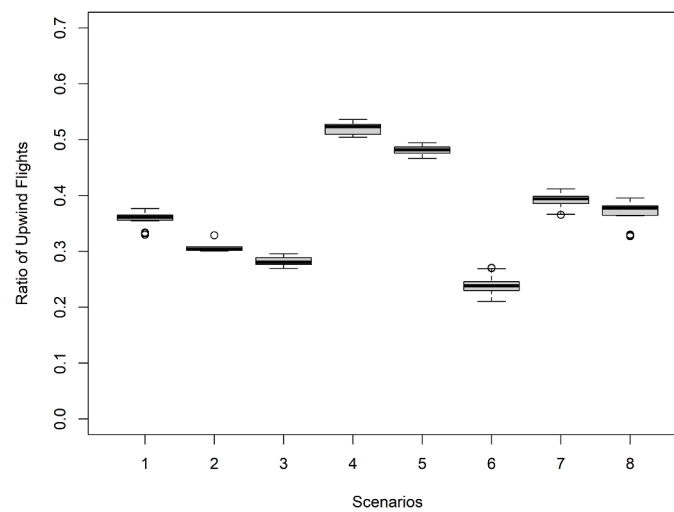
Appendix D

(Fig. D-1)

Fig. D-1. Ratio of number of upwind flights over the total number of flights performed by simulated swarms of each scenarios with the optimised parameter set (Compr. PUF).

Appendix E

To illustrate further the better quality of the reproduction of migration pathways with the PUF version of the model**, we produce here the same maps as** Figs. 3**and** 4 **and** Appendices B **and** C **for the IUF model version**. The Compr. IUF parameterisation (Table 4) was used. Note that the initial swarm number was the same: 50/replicate. However, the lack of mobility of swarms in this version of the model did reduce the swarm number in some scenarios when swarms did not find enough food (and reduced in size by cannibalism until "dying" in the simulations). This is particularly the case in Scenario 1 (Figs. E-1-E-8)
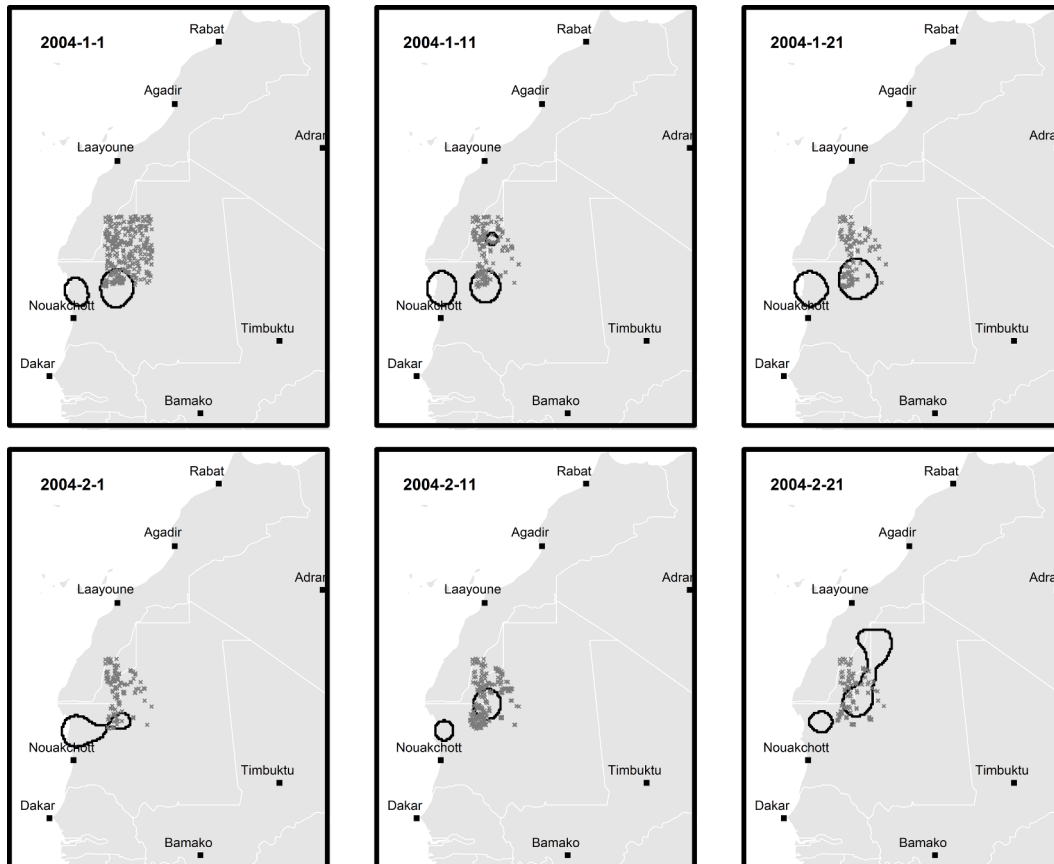

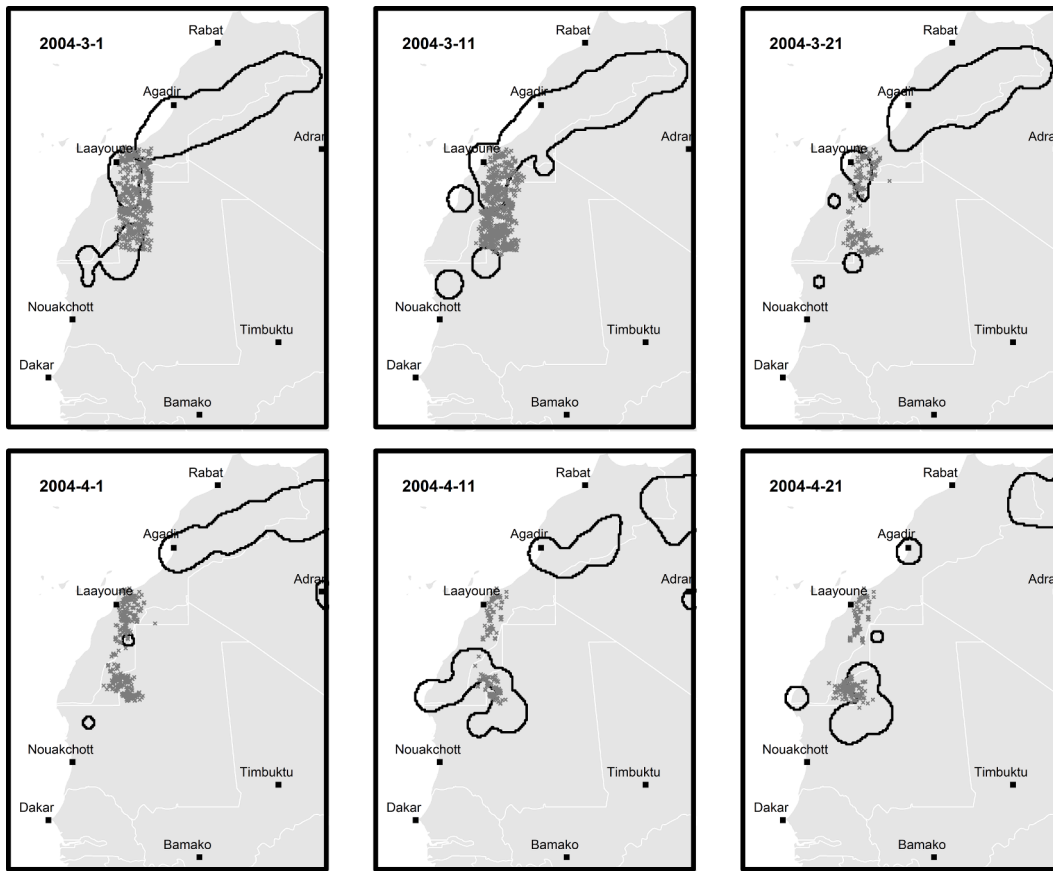**Fig. E-1.** Scenario 1, Jan.-Feb. 2004.
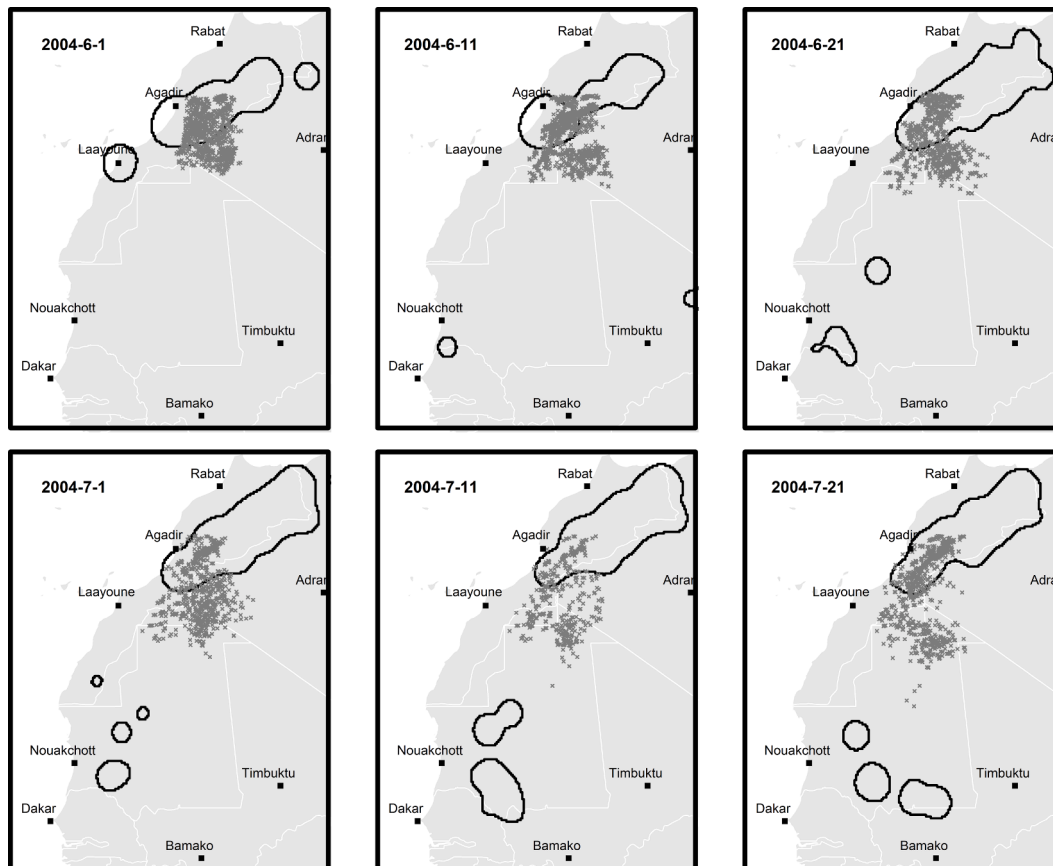
Fig. E-2. Scenario 2, Mar.-Apr. 2004.

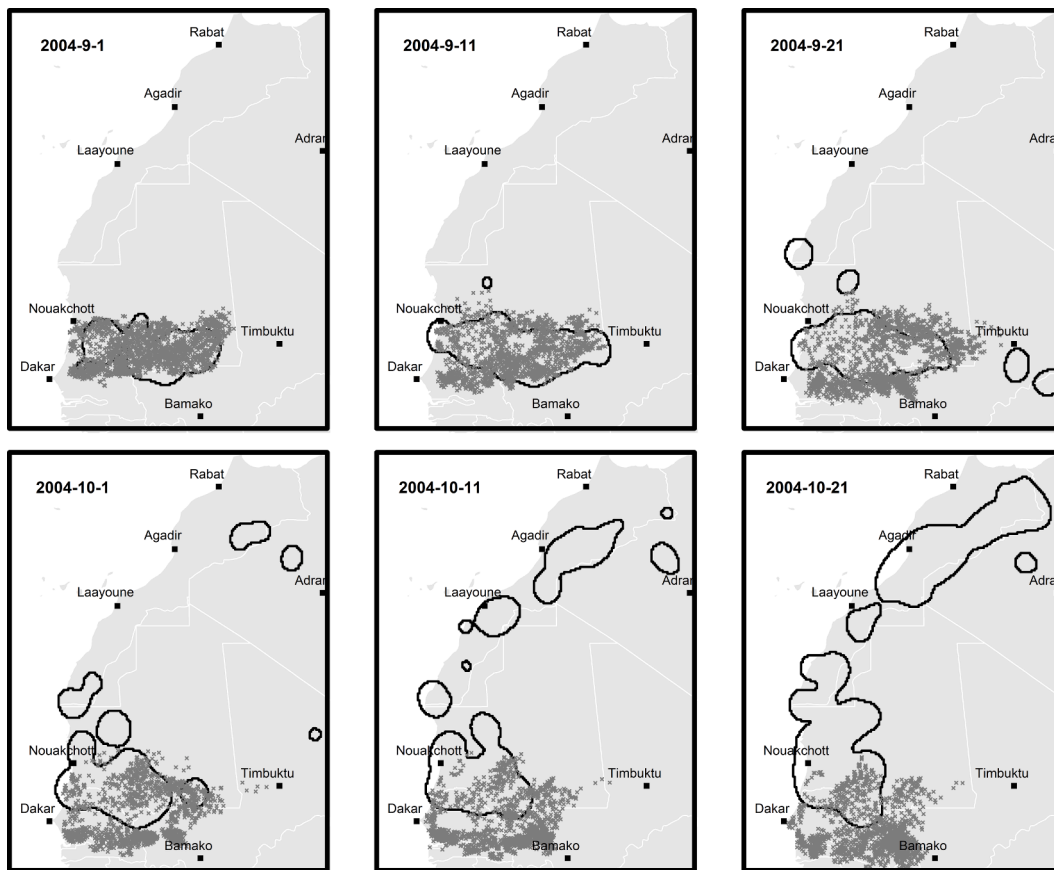**Fig. E-3.** Scenario 3, Jun.-Jul. 2004.

Fig. E-4. Scenario 4, Sep.-Oct. 2004.

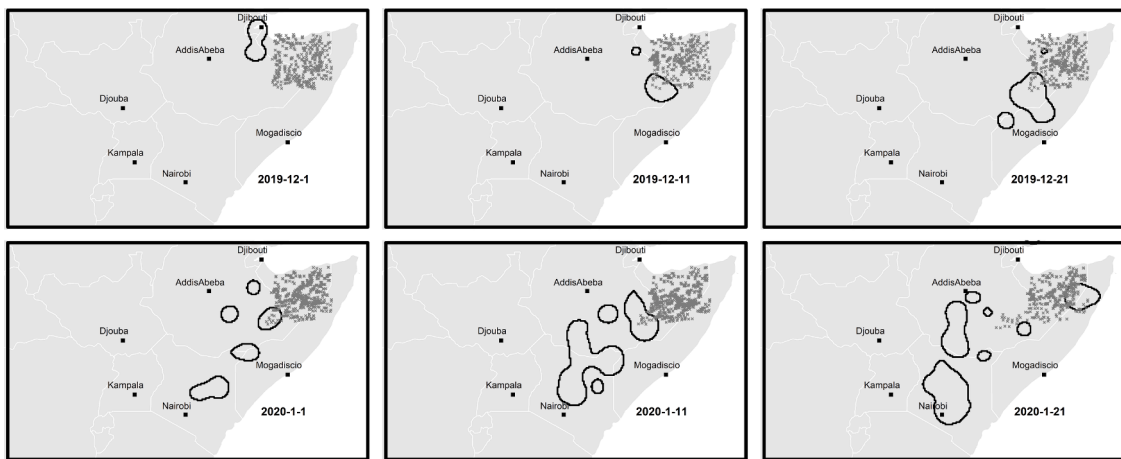**Fig. E-5.** Scenario 5, Oct.-Nov. 2019.

Fig. E-6. Scenario 6, Dec. 2019-Jan. 2020.

Fig. E-7. Scenario 7, Feb.-Mar. 2020.

Fig. E-8. Scenario 8, Apr.-May 2020.

References

Ariel, G., Ayali, A., 2015. Locust collective motion and its modeling. PLoS Comput. Biol. 11, e1004522 https://doi.org/10.1371/journal.pcbi.1004522.

Baddeley, A., Ege, R., Rolf, T., 2015. Spatial Point Patterns: Methodology and Applications with R. Chapman & Hall /CRC Press, London. https://www.routledge.com/Spatial-Point-Patterns-Methodology-and-Applications-with-R/Baddeley-Rubak-Turner/p/book/9781482210200 [Accessed 2023/01/23].

Cary, J.R., Small, R.J., Rusch, D.H., 1992. Dispersal of ruffed grouse: a large-scale individual-based model. In: McCullough, DR, Barrett, RH (Eds.), Wildlife 2001: Populations. Springer Netherlands, Dordrecht, pp. 727–737. https://doi.org/10.1007/978-94-011-2868-1_54.

Ceccato, P., Cressman, K., Giannini, A., Trzaska, S., 2007. The desert locust upsurge in West Africa (2003-2005): information on the desert locust early warning system and the prospects for seasonal climate forecasting. Int. J. Pest. Manag. 53 (1), 7–13. https://doi.org/10.1080/09670870600968826.

Cissé, S., Ghaout, S., Mazih, A., Ould Babah, M.A., Sidi Benahi, A., Piou, C., 2013. Effect of vegetation on density thresholds of Desert locust gregarization from survey data in Mauritania. Entomol. Exp. Appl. 146, 156–165. https://doi.org/10.1111/eea.12121.

Collett, M., Despland, E., Simpsom, S.J., Krakauer, D.C., 1998. Spatial scales of Desert locust gregarization. Proc. Natn Acad. Sci. USA 95, 13052–13055. https://doi.org/10.1073/pnas.95.22.13052.

Cressman, 2008. The use of new technologies in desert locust early warning. Outlook. Pest Manag. 19 (2), 55–59. https://doi.org/10.1564/19apr03.

Cressman, K., 2013. Role of remote sensing in desert locust early warning. J. Appl. Remote Sens. 7 (1), 075098 https://doi.org/10.1117/1.JRS.7.075098.

Cressman, K., Stefanski, R., 2016. *Weather and Desert Locusts*. **WMO-1175**. World Meteorological Organization & Food and Agriculture Organization of the United Nations, Geneva & Rome, p. 38. https://library.wmo.int/doc_num.php?explnum_id=3213 [Accessed 2023/01/23].

Davey, 1954. Quantities of food eaten by the desert locust, *Schistocerca gregaria* (Forsk.), in relation to growth. Bull. Entomol. Res. 45, 539–551. https://doi.org/10.1017/S0007485300029618.

Didan, K., Barreto Munoz, A., Huete, A., 2015. Modis Vegetation Index User's Guide (MOD13 Series). Vegetation Index and Phenology Lab: The University of Arizona, p. 32. https://vip.arizona.edu/documents/MODIS/MODIS_VI_UsersGuide_June_2015_C6.pdf [Accessed 2023/01/23].

Dkhili, J., Berger, U., Idrissi Hassani, L.M., Ghaout, S., Peters, R., Piou, C., 2017. Self-organized spatial structures of locust groups emerging from local interaction. Ecol. Modell. 361, 26–40. https://doi.org/10.1016/j.ecolmodel.2017.07.020.

Draper, J., 1980. The direction of Desert Locust migration. J. Anim. Ecol. 49 (3), 959–974. https://doi.org/10.2307/4238.

Edelstein-Keshet, L., Watmough, J., Grunbaum, D., 1998. Do travelling band solutions describe cohesive swarms? An investigation for migratory locusts. J. Math. Biol. 36 (6), 515–549. https://doi.org/10.1007/s002850050112.

Edmonds, B., Moss, S., 2004. From KISS to KIDS – An 'anti-simplistic'modelling approach. In: International workshop on multi-agent systems and agent-based simulation. Springer, pp. 130–144. https://doi.org/10.1007/978-3-540-32243-6_11.

Elagba, M., 2015. Determination of nutritive value of the edible migratory locust *Locusta migratoria* (Linnaeus, 1758) (Orthoptera: Acrididae). Int. J. Adv. Pharm. Biol. Chem. 4, 144–148. http://api.uofk.edu:8080/api/core/bitstreams/ac3cf842-bdbe-4a0e-b546-57acd1a0c03d/content [Accessed 2023/01/23].

FAO, n.d.1. *Climate Change and Desert Locust*. Locust Watch/Desert Locust, https://www.fao.org/ag/locusts/en/activ/1307/climate/index.html [Accessed 2022/04/05].

FAO, n.d.2. *Desert Locust upsurge in 2004-2005*. Locust Watch/Desert Locust, https://www.fao.org/ag/locusts/en/archives/1146/web04/index.html [Accessed 2022/10/25].

FAO, 2004. Desert Locust Bulletin, 313. FAO Emergency Centre for Locust Operations, Rome, p. 9. https://reliefweb.int/report/algeria/desert-locust-bulletin-313-october-2004-enar [Accessed 2023/01/23].

FAO, 2022. *Technical Guidance On Desert locust. Early warning System and Sustainable Management of Transboundary pests, With Special Reference to Desert Locust* (Schistocerca Gregaria *[Forskål])* in South Asia. FAO, Bangkok, p. 41. https://www.fao.org/3/cc0147en/cc0147en.pdf [Accessed 2023/01/12].

Gay, P.E., Truper, E.V., Piou, C., 2021. Importance of human capital, field knowledge and experience to improve pest locust management. Pest Manag. Sci. 77 (12), 5463–5474. https://doi.org/10.1002/ps.6587.

Gelaro, R., McCarty, W., Suarez, M.J., Todling, R., Molod, A., Takacs, L., Randles, C.A., Darmenov, A., Bosilovich, M.G., Reichle, R., Wargan, K., Coy, L., Cullather, R., Draper, C., Akella, S., Buchard, V., Conaty, A., da Silva, A.M., Gu, W., Kim, G.K., Koster, R., Lucchesi, R., Merkova, D., Nielsen, J.E., Partyka, G., Pawson, S., Putman, W., Rienecker, M., Schubert, S.D., Sienkiewicz, M., Zhao, B., 2017. The modern-era retrospective analysis for research and applications, version 2 (MERRA-2). J. Clim. 30, 5419–5454. https://doi.org/10.1175/JCLI-D-16-0758.1.

Grimm, V., Ayllón, D., Railsback, S.F., 2017. Next-generation individual-based models integrate biodiversity and ecosystems: yes we can, and yes we must. Ecosystems 20, 229–236. https://doi.org/10.1007/s10021-016-0071-2.

Grimm, V., Berger, U., Bastiansen, F., Eliassen, S., Ginot, V., Giske, J., et al., 2006. A standard protocol for describing individual-based and agent-based models. Ecol. Modell. 198, 115–126. https://doi.org/10.1016/j.ecolmodel.2006.04.023.

Grimm, V., Berger, U., DeAngelis, D.L., Polhill, J.G., Giske, J., Railsback, S.F., 2010. The ODD protocol: a review and first update. Ecol. Modell. 221, 2760–2768. https://doi.org/10.1016/j.ecolmodel.2010.08.019.

Grimm, V., Railsback, S.F., Vincenot, C.E., Berger, U., Gallagher, C., DeAngelis, D.L., Edmonds, B., Geh, J., Giskei, J., Groeneveldj, J., Johnstonk, A.S.A., Millesa, A., Nabe-Nielsene, J., Polhilll, J.G., Radchukm, V., Rohwädern, M.S., Stillmano, R.A., Thielep, J.C., Ayllón, D., 2020. The ODD protocol for describing agent-based and other simulation models: a second update to improve clarity, replication, and structural realism. J. Artifi. Soci. Soc. Simulat. 23, 7. https://doi.org/10.18564/jasss.4259.

Grimm, V., Revilla, E., Berger, U., Jeltsch, F., Mooij, W.M., Railsback, S.F., Thulke, H.H., Weiner, J., Wiegand, T., DeAngelis, D.L., 2005. Pattern-oriented modeling of agent-based complex systems: lessons from ecology. Science 310 (5750), 987–991. https://doi.org/10.1126/science.1116681.

Gómez, D., Salvador, P., Sanz, J., Casanova, C., Taratiel, D., Casanova, J.L., 2019. Desert locust detection using Earth observation satellite data in Mauritania. J. Arid Environ. 164, 29–37. https://doi.org/10.1016/j.jaridenv.2019.02.005.

Huston, M., DeAngelis, Post, W., 1988. New computer models unify ecological theory: computer simulations show that many ecological patterns can be explained by interactions among individual organisms. Bioscience 38, 682–691. https://doi.org/10.2307/1310870.

Katel, S., Raj Mandal, H., Neupane, P., Timsina, S., Pokhrel, P., Katuwal, A., Subedi, S., Shrestha, J., Kumari Shah, K., 2021. Desert Locust (*Schistocerca gregaria* Forskål) and its management: a review. J. Agricult. Appl. Biol. 2 (1), 61–69. https://doi.org/10.11594/jaab.02.01.08.

Kennedy, J.S., 1951. The migration of the Desert locust (*Schistocerca gregaria* Forsk.). I. The behaviour of swarms. II. A theory of long-range migrations. Biolog. Sci. Rev. 235 (625), 163–290. https://doi.org/10.1098/rstb.1951.0003.

Kooijman, S.A.L.M., Sousa, T., Pecquerie, L., van der Meer, J., Jager, T., 2008. From food-dependent statistics to metabolic parameters, a practical guide to the use of dynamic energy budget theory. Biol. Rev. 83, 533–552. https://doi.org/10.1111/j.1469-185X.2008.00053.x.

Kooijman, S.A.L.M., 2009. Dynamic Energy Budget Theory For Metabolic Organisation, 3rd ed. Cambridge University Press, p. 489. https://doi.org/10.1017/CBO9780511805400.

Kouřimskáá, L., Adámkováb, A., 2016. Nutritional and sensory quality of edible insects. NFS J. 4, 22–26. https://doi.org/10.1016/j.nfs.2016.07.001.

Kritsky, G., 1997. The insects and other arthropods of the Bible, the new revised version. Am. Entomolog. 43, 183–188. https://doi.org/10.1093/ae/43.3.183.

Maeno, K., Ould Ely, S., Ould Mohamed, S.A., Jaavar, M.E.H., Ould Babah Ebbe, M.A., 2020. Adult Desert Locust swarms, *Schistocerca gregaria*, preferentially roost in the tallest plants at any given site in the Sahara Desert. Agronomy 10 (12), 1–17. https://doi.org/10.3390/agronomy10121923, 1923.

Magor, J.I., Lecoq, M., Hunter, D.M., 2008. Preventive control and Desert Locust plagues. Crop Prot. 27 (12), 1527–1533. https://doi.org/10.1016/j.cropro.2008.08.006.

Mariod, A.A., 2020. Nutrient composition of Desert Locust (*Schistocerca gregaria*). In: Mariod, AA (Ed.), African Edible Insects As Alternative Source of food, oil, Protein and Bioactive Components. Springer, Cham, pp. 257–263. https://doi.org/10.1007/978-3-030-32952-5_18.

Meneses-Tovar, 2011. NDVI As Indicator of Degradation, 62. Revista Internacional de Silvicultura e Industrias Forestales, Unasylva, p. 8. https://www.fao.org/3/i2560e/i2560e07.pdf [Accessed 2023/01/23].

Meynard, C.N., Gay, P.E., Lecoq, M., Foucart, A., Piou, C., Chapuis, M.P., 2017. Climate-driven geographic distribution of the Desert locust during recession periods: subspecies' niche differentiation and relative risks under scenarios of climate change. Glob. Chang. Biol. 23 (11), 4739–4749. https://doi.org/10.1111/gcb.13739.

Meynard, C.N., Lecoq, M., Chapuis, M.P., Piou, C., 2020. On the relative role of climate change and management in the current Desert Locust outbreak in East Africa. Glob. Chang. Biol. 1–3. https://doi.org/10.1111/gcb.15137.

Murakami, H., Niizato, T., Gunji, Y.P., 2017. Emergence of a coherent and cohesive swarm based on mutual anticipation. Sci. Rep. 7 (46447), 1–9. https://doi.org/10.1038/srep46447.

O'Neill, B., 2020. Locust Hub dataset, Adults. Food and Agriculture Organization of the United Nations, Rome. https://locust-hub-hqfao.hub.arcgis.com/datasets/adults/explore?location=10.919983%2C-0.866667%2C3.06 [Accessed 2022/03/14].

Parry, H.R., Bithell, M., 2012. Large scale agent-based modelling: a review and guidelines for model scaling. In: Heppenstall, AJ, Crooks, AT, See, LM, Batty, M. (Eds.), Agent-Based Models of Geographical Systems. Springer Netherlands, Dordrecht, pp. 271–308. https://doi.org/10.1007/978-90-481-8927-4_14.

Pener, M.P., Simpson, S.J., 2009. Locust phase polyphenism: an update. Adv. Insect Physiol. 36, 1–272. https://doi.org/10.1016/S0065-2806(08)36001-9.

Pettorelli, N., Ryan, S., Mueller, T., Bunnefeld, N., Jedrzejewska, B., Lima, M., Kausrud, K., 2011. The normalized difference vegetation index (NDVI): unforeseen successes in animal ecology. Clim. Res. 46, 15–27. https://doi.org/10.3354/cr00936.

Pélissié, B., Piou, C., Jourdan-Pineau, H., Pagès, C., Blondin, L., Chapuis, M.P., 2016. Extra molting and selection on nymphal growth in the desert locust. PLoS One 11, e0155736. https://doi.org/10.1371/journal.pone.0155736.

Piou, C., Lebourgeois, V., Benahi, A.S., Bonnal, V., Jaavar, M.E.H., Lecoq, M., Vassal, J. M., 2013. Coupling historical prospection data and a remotely-sensed vegetation index for the preventative control of Desert locusts. Basic Appl. Ecol. 14 (7), 593–604. https://doi.org/10.1016/j.baae.2013.08.007.

Piou, C., Jaavar Bacar, M.E.H., Babah Ebbe, M.A., Chihrane, J., Ghaout, S., Cissé, S., Lecoq, M., Ben Halima, T., 2017. Mapping the spatiotemporal distributions of the Desert Locust in Mauritania and Morocco to improve preventive management. Basic Appl. Ecol. 25, 37–47. https://doi.org/10.1016/j.baae.2017.10.002.

Piou, C., Gay, P.E., Benahi, A.S., Ould Babab Ebbe, M.A., Chihrane, J., Ghaout, S., Cissé, S., Diakité, F., Lazar, M., Cressman, K., Merlin, O., Escorihuela, M.J., 2019. Soil moisture from remote sensing to forecast Desert locust presence. J. Appl. Ecol. 56 (4), 966–975. https://doi.org/10.1111/1365-2664.13323.

Piou, C., Marescot, L., 2023. Spatiotemporal risks forecasting to improve locust management. Curr. Opin. Insect Sci. 56, 101024 https://doi.org/10.1016/j.cois.2023.101024.

Rainey, R.C., 1963. Meteorology and the migration of desert locusts. Applications of synoptic meteorology in locust control. Anti-Locust Memoir 7, 1–117.

Rainey, R.C., Waloff, Z., 1951. Flying locusts and convection currents. Anti-Locus. Bullet. 9, 51–72.

Roffey, J., Magor, J.I., 2003. *Desert Locust Population parameters*. Coll.: "Desert Locust Field Research stations, Technical Series", 29. FAO, Rome. V +.

Roffey, J., Popov, G.B., 1968. Environmental and behavioural processes in a Desert locust outbreak. Nature 219 (5133), 446–450. https://doi.org/10.1038/219446a0.

Rohde, R.A., Hausfather, Z., 2020. The Berkeley earth land/ocean temperature record. Earth Syst. Sci. Data 12, 3469–3479. https://doi.org/10.5194/essd-12-3469-2020.

Romanczuk, P., Couzin, I.D., Schimansky-Geier, L., 2009. Collective motion due to individual escape and pursuit response. Phys. Rev. Lett. 102, 010602 https://doi.org/10.1103/PhysRevLett.102.010602.

Roujean, J.L., Leon-Tavares, J., Smets, B., Claes, P., Camacho de Coca, F., Sanchez-Zapero, J., 2018. Surface albedo and toc-r 300 m products from proba-v instrument in the framework of Copernicus global land service. Remote Sens. Environ. 215 (15), 57–73. https://doi.org/10.1016/j.rse.2018.05.015.

Shashar, N., Sabbah, S., Aharoni, N., 2005. Migrating locusts can detect polarized reflections to avoid flying over the sea. Biol. Lett. 1 (4), 472–475. https://doi.org/10.1098/rsbl.2005.0334.

Showler, A.T., 2003. The importance of armed conflict to desert locust control, 1986-2002. J. Orthoptera Res. 12, 127–133. https://doi.org/10.1665/1082-6467(2003)012[0127:TIOACT]2.0.CO;2.

Stein, A.F., Draxler, R.R., Rolph, G.D., Stunder, B.J.B., Cohen, M.D., Ngan, F., 2015. NOAA's HYSPLIT atmospheric transport and dispersion modeling system. Bull. Am. Meteorol. Soc. 96 (12), 2059–2077.

The R Project for Statistical Computing (n.d.) [Website]. https://www.r-project.org [Accessed 2022-03-31].

Sultana, R., Kumar, S., Samejo, A.A., Soomro, S., Lecoq, M., 2021. The 2019-2020 upsurge of the desert locust and its impact in Pakistan. J. Orthoptera Res. 30 (2), 145–154. https://doi.org/10.3897/jor.30.65971.

Symmons, P.M., Cressman, K., 2001. Desert Locust Guidelines. 1. Biology and Behaviour. FAO, Rome, p. 43. https://www.fao.org/ag/locusts/common/ecg/347_en_DLG1e.pdf [Accessed 2023/01/23].

Topaz, C.M., Bernoff, A.J., Logan, S., Toolson, W., 2008. A model for rolling swarms of locusts. Europ.Phys.J.special Top. 157, 93–109. https://doi.org/10.1140/epjst/e2008-00633-y.

Topaz, C.M., D'Orsogna, M.R., Edelstein-Keshet, L., Bernoff, A.J., 2012. Locust dynamics: behavioral phase change and swarming. PloS Comput.Biol 8, 1–11. https://doi.org/10.1371/journal.pcbi.1002642.

Uvarov, B.P., 1944. The locust plague. J. Econ. Entomol. 37, 93–99. https://doi.org/10.1093/jee/37.1.93.

Uvarov, B.P., 1977. Grasshoppers and locusts. A handbook of General acridology. II: Behaviour, ecology, biogeography, Population Dynamics. Centre for Overseas Pest Research, London, p. 613. IX +.

Van der Meer, J., 2006. An introduction to Dynamic Energy Budget (DEB) models with special emphasis on parameter estimation. J. Sea Res. 56 (2), 85–102. https://doi.org/10.1016/j.seares.2006.03.001.

van Huis, A., Woldewahid, G., Toleubayev, K., van der Werf, W., 2008. Relationships between food quality and fitness in the desert locust, *Schistocerca gregaria*, and its distribution over habitats on the red sea coastal plain of Sudan. Entomol. Exp. Appl. 127 (2), 144–156. https://doi.org/10.1111/j.1570-7458.2008.00682.x.

Van Huis, A., van Itterbeek, J., Klunder, H., Mertens, E., Halloran, A., Muir, A., Vantomme, P., 2013. *Edible insects: Future Prospects For Food and Feed security*. FAO Forestry Papers, **171**. Food and Agriculture Organization of the United Nations, Rome, Italy, p. 187. https://doi.org/10.1016/j.jfutfo.2021.10.001.

Waloff, Z., 1966. The upsurges and recessions of the Desert Locust plague: an historical survey. Anti-Locust Memoir 8, 1–111.

Waloff, Z., 1972. Observations on the airspeeds of freely flying locusts. Anim. Behav. 20, 367–372.

Waloff, Z., Rainey, R.C., 1951. Field studies on factors affecting the displacements of Desert locust swarms in Eastern Africa. Anti-Locust Bulletin 9, 1–50.

Weis-Fogh, T., 1952. Fat combustion and metabolic rate of flying locusts (*Schistocerca gregaria* Forskål). Philosoph. Transact. Roy. Soc. Lond., B 640 (237), 1–36. https://doi.org/10.1098/rstb.1952.0011.

Weis-Fogh, T., 1956. Biology and physics of locust flight. II. Flight performance of the Desert locust (*Schistocerca gregaria* Forskål). *Philosoph. Transact. Roy. Soc. Lond., B* 667 (239), 459–510.

Wilensky, U., 1999. *NetLogo* [Website]. Center for Connected Learning and Computer-Based Modeling, Northwestern University, Evanston, IL. https://ccl.northwestern.edu/netlogo/ [Accessed 2022/03/14].

Yates, C.A., Erban, R., Escudero, C., Couzin, I.D., Buhl, J., Kevrekidi, I.G., Maini, P.K., Sumpter, D.V.T., 2009. Inherent noise can facilitate coherence in collective swarm motion. Proc. Natl Acad. Sci. 106 (14), 5454–5469. https://doi.org/10.1073/pnas.0811195106.